THE JOURNAL OF BIOLOGICAL CHEMISTRY VOL. 291, NO. 21, pp. 10986–11002, May 20, 2016
© 2016 by The American Society for Biochemistry and Molecular Biology, Inc. Published in the U.S.A.

Actin-Sorting Nexin 27 (SNX27)-Retromer Complex Mediates Rapid Parathyroid Hormone Receptor Recycling*[S]

Received for publication, October 7, 2015, and in revised form, March 22, 2016 Published, JBC Papers in Press, March 23, 2016, DOI 10.1074/jbc.M115.697045

Jennifer C. McGarvey[‡], Kunhong Xiao[‡], Shanna L. Bowman[§], Tatyana Mamonova[‡], Qiangmin Zhang[‡], Alessandro Bisello[‡], W. Bruce Sneddon[‡], Juan A. Ardura[‡1], Frederic Jean-Alphonse[‡], Jean-Pierre Vilardaga[‡], Manojkumar A. Puthenveedu[§], and Peter A. Friedman[‡¶2]

From the [‡]Laboratory for GPCR Biology, Department of Pharmacology and Chemical Biology, and the [¶]Department of Structural Biology, University of Pittsburgh School of Medicine, Pittsburgh, Pennsylvania 15261 and the [§]Department of Biological Sciences, Carnegie Mellon University, Pittsburgh, Pennsylvania 15213

The G protein-coupled parathyroid hormone receptor (PTHR) regulates mineral-ion homeostasis and bone remodeling. Upon parathyroid hormone (PTH) stimulation, the PTHR internalizes into early endosomes and subsequently traffics to the retromer complex, a sorting platform on early endosomes that promotes recycling of surface receptors. The C terminus of the PTHR contains a type I PDZ ligand that binds PDZ domain-containing proteins. Mass spectrometry identified sorting nexin 27 (SNX27) in isolated endosomes as a PTHR binding partner. PTH treatment enriched endosomal PTHR. SNX27 contains a PDZ domain and serves as a cargo selector for the retromer complex. VPS26, VPS29, and VPS35 retromer subunits were isolated with PTHR in endosomes from cells stimulated with PTH. Molecular dynamics and protein binding studies establish that PTHR and SNX27 interactions depend on the PDZ recognition motif in PTHR and the PDZ domain of SNX27. Depletion of either SNX27 or VPS35 or actin depolymerization decreased the rate of PTHR recycling following agonist stimulation. Mutating the PDZ ligand of PTHR abolished the interaction with SNX27 but did not affect the overall rate of recycling, suggesting that PTHR may directly engage the retromer complex. Coimmunoprecipitation and overlay experiments show that both intact and mutated PTHR bind retromer through the VPS26 protomer and sequentially assemble a ternary complex with PTHR and SNX27. SNX27-independent recycling may involve *N*-ethylmaleimide-sensitive factor, which binds both PDZ intact and mutant PTHRs. We conclude that PTHR recycles rapidly through at least two pathways, one involving the ASRT complex of actin, SNX27, and retromer and another possibly involving *N*-ethylmaleimide-sensitive factor.

G protein-coupled receptors (GPCRs)[3] constitute the most abundant family of cell surface transmembrane receptors that activate intracellular signaling pathways in response to extracellular stimuli. These receptors typically behave in a cyclical pattern of activation and inactivation, where receptor desensitization guards cells against excessive stimulation, and resensitization protects cells against prolonged resistance to stimuli. Following ligand binding, GPCRs undergo desensitization and internalization and then either recycling to the plasma membrane or degradation by the lysosome or proteasome (1). Critical steps controlling the fate of internalized GPCRs occur in endosomes, where exposure to low pH facilitates ligand-receptor dissociation with the subsequent sorting to a recycling pathway that returns the receptor to the cell surface or to a degradative pathway. These unidirectional processes are thought to be determined mainly by accessory proteins and post-translational modifications (2). The actin-sorting nexin 27-retromer tubule (ASRT) complex is a multiprotein assembly that forms a major sorting platform on early endosomes (3). This complex assembles retromer-positive tubules on early endosomes, from which cargo vesicles transport membrane proteins to the plasma membrane or Golgi apparatus in an actin-dependent manner (4–6). Retromer itself is composed of a VPS26-VPS29-VPS35 ternary complex that interacts with cargo proteins and two BAR (Bin-amphiphysin-Rvs) domain-containing sorting nexins, which localize the complex to endosomes and are thought to participate in tubule formation (6–9). Recycling by the ASRT complex depends on actin and is mediated by the Wiskott-Aldrich syndrome protein and scar homologue (WASH) complex, an activator of the actin nucleator Arp2/3 (10, 11) that is recruited to endosomes by retromer and is required for vesicle budding from the endosomal tubule to return cargo to the cell surface (12, 13).

* This work was supported by National Institutes of Health Grants DK069998, DK054171, and DK105811 (to P. A. F.); DK087688 and GM117425 (to M. A. P.); and DK102495 (to J. P. V.). This work was also supported by National Science Foundation Grant 1517776 (to M. A. P.). The authors declare that they have no conflicts of interest with the contents of this article. The content is solely the responsibility of the authors and does not necessarily represent the official views of the National Institutes of Health.

[S] This article contains supplemental Figs. 1–6.

[1] Present address: School of Medicine, San Pablo CEU University, 28668 Madrid, Spain.

[2] To whom correspondence should be addressed: University of Pittsburgh School of Medicine, Dept. of Pharmacology and Chemical Biology, E1356 Thomas E. Starzl Biomedical Science Tower, 200 Lothrop St., Pittsburgh, PA 15261. E-mail: paf10@pitt.edu.

[3] The abbreviations used are: GPCR, G protein-coupled receptor; SNX27, sorting nexin 27; ASRT, actin-sorting nexin 27-retromer tubule complex; WASH, Wiskott-Aldrich syndrome protein and scar homologue; PDZ, postsynaptic density 95/disc large/zona occludens; PNS, post-nuclear supernatant; FERM, 4.1 protein, ezrin, radixin, and moesin; VPS, vacuolar protein-sorting protein; β_2AR, β_2-adrenergic receptor; PTHR, parathyroid hormone receptor; NHERF1, Na^+/H^+ exchanger regulatory factor; SEP, superecliptic pHluorin; TIRF, total internal reflection fluorescence; LatA, latrunculin A; NSF, *N*-ethylmaleimide-sensitive factor; DSP, dithiobis(succinimidyl propionate); RIPA, radioimmune precipitation assay; HBTU, *O*-(benzotriazol-1-yl)-*N*,*N*,*N*′,*N*′-tetramethyluronium hexafluorophosphate; HOBt, 1-hydroxybenzotriazole; DIEA, diisopropylethylamine.

Sorting nexins comprise a family of proteins characterized by the presence of a PX (Phox homology) domain for lipid binding. They are expressed throughout the endosomal system, where they participate in multiple trafficking pathways (14). Sorting nexin 27 (SNX27) is the only member containing a PDZ (postsynaptic density 95/disc large/zona occludens) domain and is one of only three sorting nexins that harbors an atypical FERM-like domain (15). The PDZ domain of SNX27 is unusual in that it contains a 13-amino acid loop that facilitates its interaction with the VPS26 domain of the retromer complex, allowing SNX27 to bind simultaneously both a cargo protein, by virtue of its PDZ domain, and retromer (16, 17). SNX27 is involved in the internalization and intracellular trafficking of β_1-adrenergic receptor, β_2-adrenergic receptor (β_2AR), SSTR5 somatostatin receptor, and metabotropic glutamate receptor 5 that harbor C-terminal PDZ ligands (4, 18–21). The β_2AR is internalized into early endosomes and sorted to actin-stabilized microdomains that regulate its recycling (22). Endosomal β_2AR sorting depends on phosphorylation and the presence of the C-terminal PDZ ligand, which promotes rapid recycling (23–25). In early endosomes, the β_2AR is recycled to the plasma membrane by the ASRT complex, which directly interacts with SNX27 (4).

The type 1 parathyroid hormone receptor (PTHR) is primarily expressed in kidney and bone, where it regulates mineral-ion homeostasis and bone turnover, respectively (26). Recycling of internalized GPCRs is categorized as rapid or slow. Class A receptors, such as the prototype β_2AR, preferentially but transiently bind β-arrestin-2, from which they rapidly dissociate, and following dephosphorylation, recycle through endosomes to the plasma membrane. Class B receptors, which include the PTHR, type 1 angiotensin II receptor, and vasopressin type 2 receptor, display similar affinities for β-arrestin-1 and β-arrestin-2, with which they remain associated, returning to the cell membrane more slowly (27, 28). It is well established that arrestin binding to many class B GPCRs, such as the type 1 angiotensin II receptor, desensitizes G protein signaling in the same manner as it does with prototype class A receptors, as with the β_2AR (29). Emerging evidence suggests that GPCRs, including peptide hormone receptors PTHR, thyroid-stimulating receptor, glucagon-like peptide 1 receptor, the pituitary adenylate cyclase-activating polypeptide type 1 receptor, and the vasopressin type 2 receptor, exhibit ligand-biased persistent G protein signaling that depends on internalization of the GPCR bound to β-arrestins (3, 30). Such β-arrestin-dependent sustained G_s interaction and cAMP signaling has been expanded to monoamine receptors, including the β_2AR and dopamine D1 receptor (31, 32).

PTHR endocytosis is mediated by clathrin in a complex with β-arrestins (33–36). PTHR and thyroid-stimulating receptor were the first mammalian GPCRs demonstrated to signal persistently through cAMP upon receptor redistribution to endosomes (37, 38). As noted above, other receptors have since been shown to behave similarly (32, 39, 40). Endosomal cAMP signaling is terminated when the acidic environment of the endosome causes ligand dissociation (41), after which the receptor interacts with the endosomal retromer complex for signal termination and subsequent trafficking (42, 43). Complete recycling of the receptor requires 1–2 h following agonist removal and before recycled receptors are able to enter a second round of internalization (34, 44).

Like other GPCRs, the intracellular regions of the PTHR are important for internalization and trafficking of the receptor and include several sites for post-translational modification and protein interactions that modulate these processes (36, 45–47). The PTHR contains a canonical class I PDZ ligand at its C terminus (48) and has a well characterized interaction with the PDZ protein Na^+/H^+ exchanger regulatory factor (NHERF1), which stabilizes the receptor at the cell membrane and links it to the actin cytoskeleton but does not affect recycling (49, 50). Here we identify SNX27 as an adaptor protein for the PTHR during endosomal sorting that promotes rapid endosome-to-plasma membrane recycling of the receptor through the ASRT complex.

Experimental Procedures

Materials—Anti-SNX27 mouse monoclonal (ab77799; 1:100 dilution for immunocytochemistry, 1:1000 for Western blotting detection) and anti-VPS35 goat polyclonal (ab10099; 1:3000 dilution) antibodies were obtained from Abcam. Anti-HA mouse monoclonal antibody and conjugated beads were obtained from Covance (HA.11[16B12]; AFC-101P-1000). Anti-HA antibody dilution was 1:2000 for immunoblotting. Anti-FLAG M2 affinity gel (A2220; 1:20 dilution for immunoprecipitation) was obtained from Sigma. Anti-Myc rabbit polyclonal (C3956; 1:1000 dilution) and anti-β-actin mouse monoclonal (A1978; 1:5000 dilution) antibodies were purchased from Sigma. AlexaFluor secondary fluorescent antibodies were obtained from Abcam (1:500 dilution). VPS26 was detected using a rabbit polyclonal anti-VPS26 antibody (Abcam, ab23892; 1:5000 dilution). Human [$Nle^{8,18}$,Tyr^{34}]PTH(1–34) was obtained from Bachem (H-9110). FuGENE 6 transfection reagent was acquired from Promega (E2691). DSP cross-linker was from CovaChem (13303-1), and latrunculin A (LatA) was from Cayman Chemical (10010630).

Cell Lines and Constructs—All experiments were performed in HEK293 cells except where indicated. Chinese hamster ovary (CHO) cells were propagated in DMEM/F-12 medium (Cellgro, 10-090CV) supplemented with 10% FBS and 1% penicillin-streptomycin.

Superecliptic pHluorin (SEP)-tagged PTHR (SEP-PTHR) was generated by large insertion PCR mutagenesis (51) using primers to amplify the SEP sequence with overhangs corresponding to the PTHR sequence at the desired insert site (forward, 5′-AAAGATAAGGCATCTGGGAAGCTCGGCGGCAGTAAAGGAGAAGAACTTTTCACT-3′; reverse, 5′-TCGGTACCTGCTGCCAGTGGGTGCGCCGCCTTTGTATAGTTCATCCATGCCATG-3′). SEP-PTHR stable cell lines were established by transfecting SEP-PTHR into HEK293 cells using FuGENE 6 and treating them with 800 μg/ml G418 to isolate single colonies, which were then propagated in 500 μg/ml G418. For isolation of endosomal PTHR, the human HA-PTHR gene was subcloned into a pACMV-tetO vector and transfected into adherent $GnTI^-$ HEK293 cells to establish a cell line stably overexpressing HA-PTHR (52). PTHR-GnTI cells were cultured in DMEM/F-12 medium (Life Technologies, 11330-032) and adapted to suspension with FreeStyle 293

medium (Invitrogen, 12238-018). The suspended cells were cultured in Erlenmeyer flasks and shaken at 120 rpm at 37 °C with 8% CO_2 before treatment. HA-PTHR expression was induced with 2 μg/ml doxycycline (Sigma, 9891) and 5 mM sodium butyrate (Sigma, B5887) for 48 h before ligand treatment. Cells were stimulated with 100 nM PTH(1–34) (hereafter referred to as PTH) for 15 min before harvesting. 120 ml of suspension cell culture were used for each experiment. SNX27 shRNA was obtained from OriGene (TF301468). Four different shRNA constructs were tested for efficiency of knockdown in HEK293 cells by immunoblotting. shRNAs F1305865 (shSNX27 865) and F1305868 (shSNX27 868) had the greatest efficiency, and these were used in subsequent experiments. The turboRFP reporter was exchanged for mCherry, which was amplified by PCR from pmCherry using primers that introduce BglII an XhoI restriction sites for insertion into pRFP-C-RS (forward, 5′-GTAAGATCTGCCACCATGGTGAGCAAGGGCGAG-3′; reverse, 5′-GCTCTCGAGTTACTTGTACAGCTCGTCCATGCC-3′). shRNA-resistant SNX27 was generated by introducing three silent mutations within the sequence targeted by shSNX27 865 using site-directed mutagenesis (forward primer, 5′-GGAGGTACAGATAACACAGTTAAGATCAGTTCCTTCTCGCCG-3′).

To create pFIV-mCherry-shVPS35, oligonucleotides were designed against the target sequence aacagtggagatattcaataa present in human, rat, and mouse VPS35. Two 5′-phosphorylated oligonucleotides (AAAGAAACAGTGGAGATATTCAATAATAGTGAAGCCACAGATGTATTATTGAATATCTCCACTGTTGG and AATTCCAACAGTGGAGATATTCAATAATACATCTGTGGCTTCACTATTATTGAATATCTCCACTGTTT) were annealed and ligated into BbsI and EcoRI-cut pFIV-mCherry. Other constructs used here have been described (17, 53–55).

Endosome Isolation—Endosomes were isolated by density gradient centrifugation. Briefly, four volumes of homogenization buffer (250 mM sucrose, 3 mM imidazole, pH 7.4, 1 mM EDTA, and protease and phosphatase inhibitors) were added to the cell pellet, which then was disrupted by Dounce homogenization on ice for ~50 strokes. The cell lysate was centrifuged at 2000 × *g* for 10 min at 4 °C. Postnuclear supernatant (PNS) was carefully transferred to a 15-ml Falcon tube, and 62% (w/w) sucrose solution (2.351 M sucrose, 3 mM imidazole, pH 7.4, 1 mM EDTA, in double-distilled H_2O; refractive index ~1.4463 at 20 °C) was added to the PNS to a final sucrose concentration of 40.6%. The diluted PNS was loaded on the bottom of an ultracentrifuge tube. 1.5 volume of 35% sucrose (1.177 M sucrose, 3 mM imidazole, pH 7.4, 1 mM EDTA, in double-distilled H_2O; refractive index ~1.3904 at 20 °C), 1 volume of 25% sucrose (0.806 M sucrose, 3 mM imidazole, pH 7.4, 1 mM EDTA, double-distilled H_2O; refractive index ~1.3723 at 20 °C), and 0.5 volume of homogenization buffer were sequentially overlaid on the top of the PNS and centrifuged at 210,000 × *g* at 4 °C for 1.5 h. The endosome fraction was collected for PTHR signaling complex isolation.

Endosomal PTHR Signaling Complex Isolation and Proteomics Analysis—1% *n*-dodecyl-β-D-maltoside was added to the endosome fraction and stirred for 1 h. The *n*-dodecyl-β-D-maltoside concentration was diluted to 0.5% before the addition of anti-HA-agarose beads (Pierce, 26181). After 4 h of incubation with agitation, the anti-HA-agarose antibody beads were collected by centrifugation, and the endosomal PTHR signaling complexes were eluted with 1 mg/ml HA peptides. The HA peptides were removed by using an Amicon Ultra 0.5-ml centrifuge filter (molecular weight cut-off 10,000; Sigma, Z677108). The endosomal PTHR signaling complexes were digested using an in-solution digestion protocol as described previously (56, 57). Tryptic peptides were subjected to LC-MS/MS analyses.

LC-MS/MS analyses were performed on a Thermo Scientific LTQ Orbitrap XL mass spectrometer with a Thermo Finnigan Nanospray II electrospray ionization source. Tryptic peptides were injected onto a 75 μm × 150-mm BEH C18 column (particle size 1.7 μm; Waters) and separated using a Waters nanoACQUITY Ultra Performance LC™ (UPLC™) system (Waters, Milford, MA) (57). The LTQ Orbitrap XL mass spectrometer was operated in the data-dependent mode using the TOP10 strategy (58). In brief, each scan cycle was initiated with a full MS scan of high mass accuracy (400–2,000 *m*/*z*; acquired by the Orbitrap XL at 6×10^4 resolution setting and automatic gain control target of 10^6), which was followed by MS/MS scans (automatic gain control target 5000; threshold 3000) in the linear ion trap on the 10 most abundant precursor ions. Selected ions were dynamically excluded for 30 s. Singly charged ions were excluded from MS/MS analysis.

MS/MS spectra were searched using the SEQUEST algorithm against a composite database containing the SwissProt *Homo sapiens* forward and reverse protein sequences. Search parameters allowed for two missed tryptic cleavages, a mass tolerance of ±10 ppm for precursor ions, a mass tolerance of ±0.02 Da for product ions, a static modification of 57.02146 Da (carboxyamidomethylation) on cysteine, and a dynamic modification of 15.99491 Da (oxidation).

Immunoprecipitation—HEK293 cells stably expressing HA-PTHR (50) were transiently transfected using FuGENE 6. 36–48 h after transfection, cells were lysed in modified RIPA buffer (1% Igepal, 0.5% sodium deoxycholate, 0.1% SDS, 10 mM Tris (pH 7.4), 150 mM NaCl, 1× protease inhibitor mixture (EMD Millipore)), and protein concentration was determined by a Bradford assay. One μg of cleared lysate was incubated overnight with anti-HA-conjugated beads at 4 °C on an orbital rotator. The following day, beads were washed four times with modified RIPA buffer, and protein was eluted in Laemmli buffer. For coimmunoprecipitation of endogenous SNX27 and VPS35, HA-PTHR HEK293 cells were treated with 25 mM DSP cross-linking reagent and incubated on ice for 2 h prior to lysis. The cross-linking reaction was terminated by a 15-min incubation with 20 mM Tris buffer, pH 7.5. Where indicated, cells were pretreated with 20 nM bafilomycin A in HEPES buffer (137 mM NaCl, 5 mM KCl, 20 mM HEPES, 1 mM $CaCl_2$, 1 mM $MgCl_2$, 0.1% (w/v) bovine serum albumin (BSA), pH 7.4) and incubated with 100 nM PTH to induce PTHR internalization.

CHO cells were used for *N*-ethylmaleimide-sensitive factor (NSF) coimmunoprecipitation because they lack NHERF1. CHO cells were transfected with FLAG-PTHR and HA-NSF constructs using LipoJet™ (SignaGen SL100468). 72 h after transfection, cells were lysed as described previously. Cell lysate

was incubated overnight with FLAG-M2 affinity gel at 4 °C. The beads were washed four times, and protein was eluted in Laemmli buffer and analyzed by immunoblotting.

Sequential immunoprecipitation was used to detect assembly of a ternary SNX27-PTHR-VPS26 complex. Six-well plates of HEK293 cells stably expressing the HA-PTHR or HA-PTHR-ETVA were transiently transfected with Myc-VPS26 and FLAG-SNX27 or the respective empty vector. After 72 h, the cells were treated with 100 nM PTH or vehicle for 5 min and then lysed with modified RIPA buffer as described above. Solubilized materials were incubated overnight at 4 °C with HA.11 monoclonal affinity matrix (Sigma, A2095). The immunoprecipitated PTHR and all interacting proteins were pelleted by spinning at 13,000 rpm for 15 min at 4 °C in an Eppendorf 5415R microcentrifuge. The pellet was washed four times in ice-cold lysis buffer and then eluted by the addition of 1 mg/ml HA peptide (Sigma, I2149) overnight. The HA beads were pelleted at 6000 rpm for 10 min, and the supernatant was transferred to a fresh tube. Myc-VPS26 was immunoprecipitated overnight with a monoclonal anti-Myc antibody (Santa Cruz Biotechnology, sc-40) and protein G Plus-agarose (Santa Cruz Biotechnology, sc-500778) at 4 °C. Immunoprecipitated FLAG-SNX27 was eluted using Laemmli sample buffer, and bound proteins were detected by immunoblotting.

Immunoblotting—Cell lysates were prepared in modified RIPA buffer, and the insoluble fraction was removed by centrifugation. The cleared lysate was diluted 1:1 in Laemmli buffer with 5% β-mercaptoethanol. Samples were electrophoresed through polyacrylamide gel and transferred to Immobilon-P membranes (Millipore) using the semidry method (Bio-Rad). Nonspecific binding was blocked by incubation in TBS-Tween with 5% powdered milk. Membranes were incubated with an appropriate primary antibody overnight at 4 °C on a shaking platform and then probed with species-specific HRP-conjugated secondary antibody. Protein was detected with ECL reagent exposed on x-ray film.

Immunocytochemistry—HEK293 cells were plated on coverslips coated with poly-D-lysine and transfected with the desired constructs. After 48 h, cells were treated with PTH and fixed in 3.6% formaldehyde. Cells were permeabilized with 0.1% Triton X-100 and incubated in 5% goat serum to block nonspecific interactions. Primary antibody was applied to the coverslips for 45 min at room temperature; cells were then rinsed in PBS and incubated in Alexa Fluor-conjugated secondary antibody for a further 45 min. Coverslips were mounted on glass microscope slides and imaged on a Nikon A1 confocal microscope. Colocalization analysis was performed using Nikon Elements software.

Molecular Dynamics Simulation—The x-ray structure of the SNX27 PDZ domain (residues 39–133) in complex with the C-terminal -ESESKV fragment of the G protein-gated inwardly rectifying potassium channel GIRK3 (Protein Data Bank code 3QGL) (59) was used as a template to build the SNX27 PDZ-PTHR complex. To model the C-terminal motif of PTHR (-EWETVM), the -ESESKV sequence was modified as follows. C-terminal Val^0 was replaced by Met, Lys^{-1} was replaced by Val, Ser^{-2} was replaced by Thr, and Ser^{-4} was replaced by Trp. His residues in the PDZ domain were treated as neutral by protonation at $N\delta^1$. The PDZ-EWETVM complex was solvated with TIP3P water molecules in a periodically replicated box (leap module of AMBER 9 (60)) and energy-minimized over 500 steps, including 100 steps of steepest descent minimization using the sander module of AMBER 9 (60). Equilibration and production simulations were then run along 20 and 80 ns, respectively.

Before equilibration simulation, the potential energy of the system was minimized by 100 steps of steepest descent minimization followed by 400 steps of conjugate gradient minimization (AMBER 11 (61)). Then a 100-ps molecular dynamics simulation was performed with protein atoms controlled in space by a harmonic restraint with a force constant of 100 kcal mol^{-1} $Å^{-2}$ to allow the water box size to shrink to its final dimensions, preventing a low water density. An isothermal isobaric ensemble (NPT) was used to adjust the solvent density (where NPT stands for number of particles, constant pressure, and temperature). The temperature of the system was gradually increased to 300 K at a constant pressure of 1 atm. Then the system was equilibrated over 100 ps in the NPT ensemble with weak restraints of 10, 5, 2, 1, and 0.1 kcal mol^{-1} $Å^{-2}$. Next, only the $C\alpha$ atoms of the N-terminal residue of the ligand were restrained with a weak force constant of 0.1 kcal mol^{-1} $Å^{-2}$ while all other atoms were free to move. The equilibration was then performed in the canonical NVT ensemble (100 ps) with a weak force constant of 0.1 kcal mol^{-1} $Å^{-2}$ (where NVT stands for number of particles, constant volume, and temperature). Production runs were then carried out for 5 ns in the NVT ensemble at 300 K using a 2-fs time step. During the production runs, the entire complex was unconstrained except for the three backbone N, C, and $C\alpha$ atoms (0.1 kcal mol^{-1} $Å^{-2}$) at the N-terminal residue of the ligand and the C-terminal residue of the protein to prevent diffusion of the complex. All simulations were performed using the AMBER 11 molecular modeling package (PMEMD module) (61) and the AMBER Parmff99SB parameter set (62). The temperature was controlled using the Berendsen thermostat (63). Periodic boundary conditions were applied. The particle mesh Ewald method (64) was used to compute long range electrostatic and Lennard-Jones interactions with 12 Å. The SHAKE algorithm was applied (65). The trajectory data were recorded at 2-ps intervals during both equilibration and production runs. Data were analyzed using the PTRAJ module in AMBER (60, 61).

Expression and Purification of SNX27 PDZ Domain—Plasmids for SNX27 PDZ(39–133) were described previously (18). The recombinant proteins were expressed in *Escherichia coli* BL21 (DE3) cells (Novagen) and purified using nickel-nitrilotriacetic acid-agarose (Qiagen) (66). The resulting proteins were divided into aliquots and stored in phosphate buffer (25 mM NaH_2PO_4, 10 mM NaCl, pH 7.4) at −80 °C until used for fluorescence polarization experiments.

Fluorescence Polarization—Fluorescence anisotropy data were obtained by increasing concentrations of the recombinant SNX27 PDZ domain in the presence of FITC-labeled PTHR peptides following the protocol described by Madden and coworkers (67). All measurements were performed in fluorescence polarization buffer (storage buffer, supplemented to a final concentration of 1 mM DTT, 0.1 mg/ml bovine IgG

(Sigma), and 0.5 mM Thesit (Fluka) containing 0.5 or 1 μM fluorescent peptide for WT or mutant systems, respectively. Polarized fluorescence intensities were measured at 25 °C with a PerkinElmer Life Sciences Wallac Victor[3] multilabel plate reader using excitation and emission wavelengths of 485 and 535 nm for FITC-labeled peptides. Anisotropy was calculated using Equation 1 from the measured fluorescence emission intensities that are polarized parallel ($I_{\parallel}$) and perpendicular ($I_{\perp}$) to the plane of the incident light (68).

$$r = I_{\parallel} - \frac{I_{\perp}}{I_{\parallel}} + 2I_{\perp} \quad \text{(Eq. 1)}$$

The equilibrium dissociation constant (K_D) for interaction between the PDZ domain and peptide was determined by fitting the fluorescent anisotropy data to Equation 2 by non-linear regression analysis and assuming formation of a 1:1 complex (68),

$$A = A_0 + \frac{K_d + [\mathrm{L}] + [\mathrm{PDZ}] - \sqrt{(K_d + [\mathrm{L}] + [\mathrm{PDZ}])^2 - 4[\mathrm{L}][\mathrm{PDZ}]}}{2[\mathrm{L}]}(A_m - A_0) \quad \text{(Eq. 2)}$$

where A is the measured anisotropy, [L] and [PDZ] are the total concentration of peptide ligand and PDZ construct, and A_0 and A_m are lower and upper anisotropy. All calculations were performed using Prism (GraphPad).

Peptide Synthesis—The PTHR C-terminal -EWETVA peptide was synthesized by solid phase methodology using standard Fmoc (*N*-[9-fluorenyl]methoxycarbonyl) chemistry (0.1-mmol scale) on an Applied Biosystems AB433 peptide synthesizer. After synthesis, the peptidyl resin was treated overnight with 4 eq of 5-(6)-carboxytetramethylrhodamine or fluorescein (FITC) in the presence of HBTU/HOBt/DIEA. Following standard trifluoroacetic acid cleavage, the product was purified by HPLC on a Vydac C-18 reverse phase column and lyophilized. The final product was characterized by electron spray mass spectrometry. The -EWETVM peptide was synthesized by the University of Pittsburgh Peptide Core Facility. FITC-labeled peptides were dissolved in PBS (storage) buffer (25 mM NaH_2PO_4, 150 mM NaCl, pH 7.4).

PTH Receptor Activity—Cyclic AMP accumulation was measured by a two-column chromatographic method described previously (50, 69).

Receptor Surface Expression—Surface expression of PTHR in HEK293 cells was measured by ELISA as described previously (47).

Live Cell PTHR Recycling—HEK293 cells stably expressing the SEP-PTHR were plated on poly-D-lysine-coated coverslips. For live imaging, cells were maintained in HEPES buffer. Confocal time lapse imaging was performed using a Nikon A1 confocal microscope with ×60, 1.4 numeric aperture objective at 37 °C. Images were acquired every 1 min. Following a 5-min baseline acquisition, 100 nM PTH was added and then washed out after 5 min.

Single Exocytic Recycling Event—Individual exocytic events were measured as described previously (70, 71). Briefly, HEK293 cells stably expressing the SEP-PTHR were plated on poly-D-lysine-coated coverslips. Cells were maintained in Leibovitz's L-15 phenol red-free medium (Gibco, 21083-027) with 10% fetal bovine serum. Total internal reflection fluorescence (TIRF) imaging was performed using a Nikon Ti microscope with a ×60, 1.49 numeric aperture TIRF objective and an ANDOR EMCCD camera. Cells were treated with 100 nM PTH for 5 min. Surface fluorescence then was bleached with high (70%) laser power and a 1-min video was acquired at 10 Hz. For actin inhibition experiments, images were recorded at 5 min after PTH application, treated with 10 mM LatA for 5 min, and then imaged for a further 1 min. Analysis of exocytosis rates was performed by counting the number of exocytic events/cell and normalizing to the cell area. The experimenter was blinded to the experimental conditions.

Blot Overlays—20 μg of VPS26, VPS29, and VPS35 protein each were separately applied to Immobilon P membranes in a volume of 100 μl using a Dot Blot Minifold Apparatus (Schleicher & Schuell Whatman, London, UK) under vacuum. The blot was blocked for 1 h with blocking buffer (TBST + 5% milk). 10 μg of HA-PTH1R-WT or HA-PTH1R-ETVA protein in blocking buffer were overlaid for 1 h at room temperature with moderate shaking. After three 10-min washes in TBST, the blot was incubated with a rabbit polyclonal anti-HA antibody (Covance) overnight at 4 °C at a 1:5000 dilution. The blot was washed four times for 10 min at room temperature in TBST and then incubated with a goat anti-mouse HRP-conjugated secondary antibody for 1 h at room temperature. After four 10-min TBST washes, the bound protein was visualized using the EMD Millipore Immobilon™ Western chemiluminescent HRP substrate. Immobilized His-VPS26 and His-VPS29 was confirmed using a monoclonal anti-His antibody (GenScript). The presence of the immobilized VPS35 was confirmed using a goat polyclonal anti-VPS35 antibody (Abcam).

Statistics—Statistical analysis was performed using GraphPad Prism version 6. Comparisons between groups were analyzed using a Mann-Whitney test, whereas repeated measures were analyzed using a paired *t* test. Differences between three or more groups were analyzed by one-way analysis of variance with post hoc testing using Dunnett's multiple comparisons test. Differences greater than $p < 0.05$ were assumed to be significant.

Results

PTHR Interacts with SNX27 in Early Endosomes—We isolated PTHR from early endosomes of HEK293 cells stably expressing HA-PTHR that were treated with 100 nM PTH for 15 min. Three fractions (F1, F2, and F3) corresponding to late endosomes, early endosomes, and Golgi/endoplasmic reticulum membranes, respectively, were purified by sucrose density gradient centrifugation (Fig. 1*A*). PTHR was detected in early endosomes (F2) and Golgi/endoplasmic reticulum membranes (F3) upon PTH exposure. PTH stimulated enrichment of PTHR in the EEA1-positive endosome F2 fraction (Fig. 1*B*). Na^+K^+-ATPase, a plasma membrane protein, was undetectable in endosomes. To identify protein adaptors that regulate post-endocytic sorting of the PTHR, the purified F2 endosomal fraction was analyzed by liquid chromatography-mass spectrometry. SNX27 was identified as an interacting protein with six peptide fragments displaying high sequence fidelity (Fig. 1*C*).

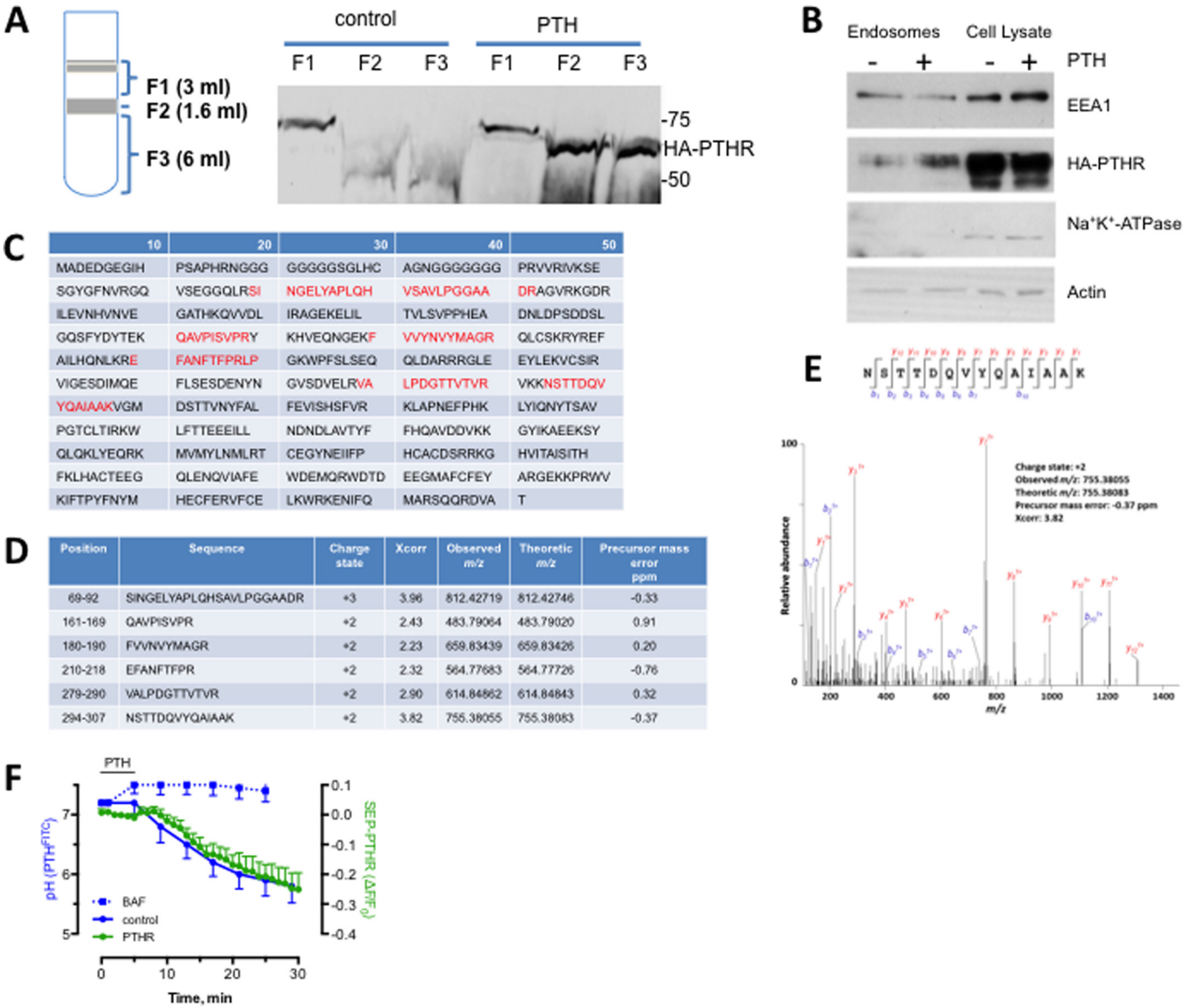

FIGURE 1. **Identification of SNX27 in endosomal PTHR signaling complexes.** SNX27 was identified in the endosomal PTHR signaling complexes by coimmunoprecipitation and LC-MS/MS analysis. After 100 nM PTH stimulation, endosomes were isolated from GnTI^{-}-HEK293 cells stably overexpressing the HA-tagged PTHR. The PTHR signaling complexes were coimmunoprecipitated from the isolated endosomes, followed by in-solution trypsin digestion and LC-MS/MS analysis. *A*, endosomes were isolated by density gradient centrifugation as outlined under "Experimental Procedures." The three fractions (*F1*, *F2*, and *F3*) correspond to late endosomes, early endosomes, and Golgi/ER membranes, respectively. PTHR was detected by immunoblotting analysis in early endosomes (*F2*) and Golgi/ER membranes (*F3*) after PTH stimulation. PTHR was not detected in the corresponding sample fractions without PTH stimulation. *B*, immunoblotting detection of PTHR in the F2 fraction of early endosome extracts from HEK293 cells expressing the HA-tagged PTHR. Autoantigen-1 (*EEA1*) served as an early endosome marker, and $Na^{+}K^{+}$-ATPase identified plasma membranes. *C*, peptides (*highlighted* in *red*) identified by LC-MS/MS analysis were mapped to the protein sequence of SNX27. *D*, position, sequence, charge state, cross-correlation (*Xcorr*), observed and theoretical *m/z*, and precursor mass error (ppm) for the identified peptides are listed. *E*, example of annotated MS/MS fragmentation spectrum for the identified peptide ^{294}NSTTDQVYQAIAAK^{307}. The *peak heights* show the relative abundances of the corresponding fragmentation ions, with the annotation of the identified matched amino terminus-containing *b* ions in *blue* and the C terminus-containing *y* ions in *red*. *F*, time-dependent changes of pH and PTHR sequestration recorded at ambient temperature using PTH^{FITC} and SEP-PTHR, respectively, in HEK293 cells. pH was calibrated using FITC fluorescence with pH standards (41). *Error bars*, S.E.

Hits were evaluated using SEQUEST cross-correlation, and scores for each SNX27 peptide fragment are shown (Fig. 1*D*) along with an example spectrum for a high scoring hit (Fig. 1*E*).

The PTHR internalizes to endosomes together with its cognate ligand (37, 41). Endosomal maturation is characterized by luminal acidification. These considerations suggested that the time course of PTHR internalization should be similar to endosomal acidification. We applied confocal microscopy to analyze the time course of PTHR endocytosis and the concurrent acidification of PTH in endosomes (Fig. 1*F*). PTHR internalization and endosomal PTH acidification commenced shortly after the addition of PTH and displayed similar half-times of about 15 min. Treatment with bafilomycin abolished acidification, verifying the endosomal location of PTHR.

SNX27 PDZ Domain Binds the PTHR C Terminus—SNX27 interaction with cargo proteins is mediated by its PDZ and by FERM-like domains (15, 18). The PTHR possesses a C-terminal PDZ ligand (-ETVM) and an upstream ezrin-binding sequence (KRK), through which it can interact directly with the FERM domain of ezrin (72, 73). Thus, the PTHR could interact with

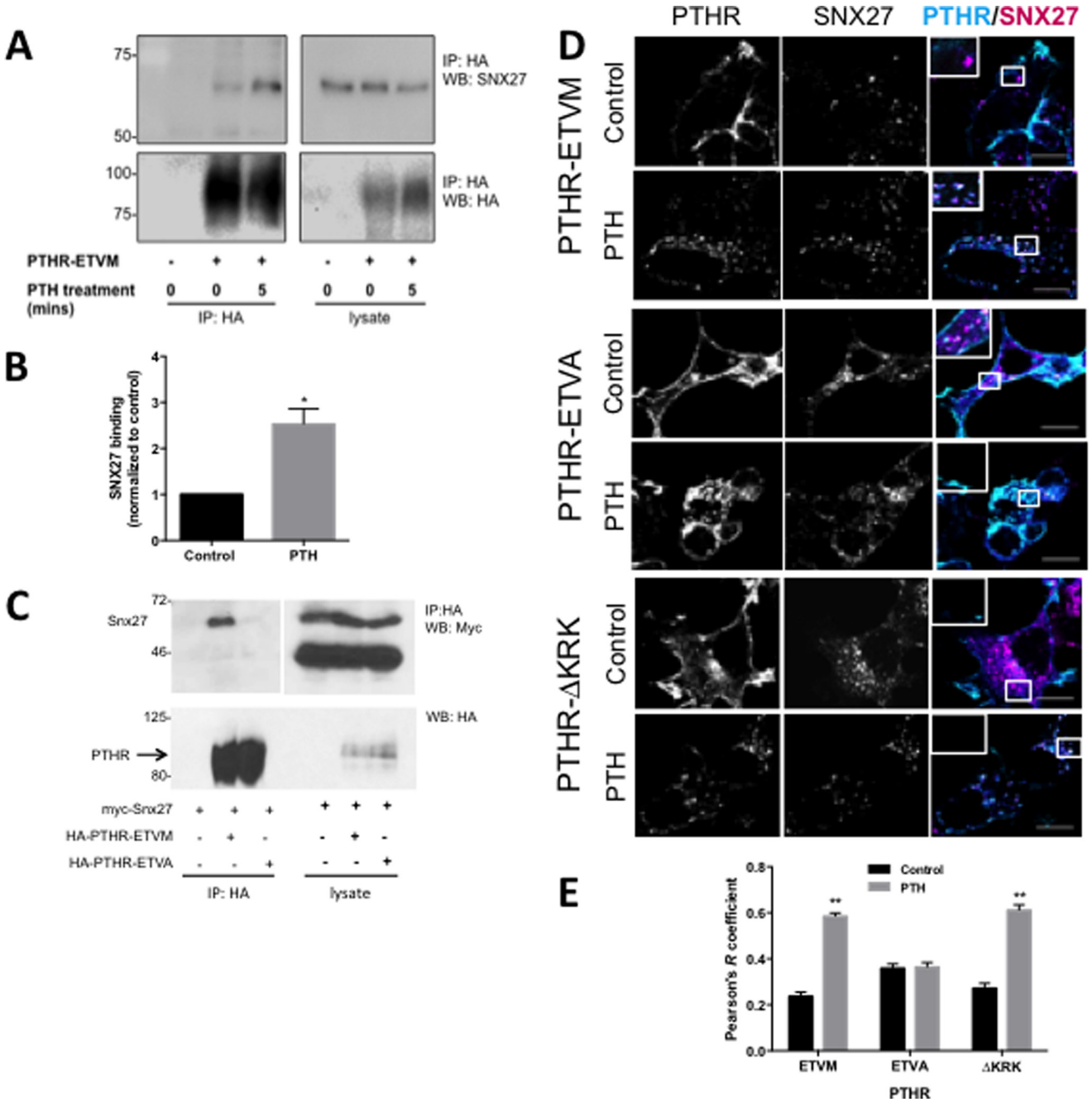

FIGURE 2. **Activation-dependent PTHR binding to SNX27 depends on PDZ interactions.** *A*, representative SNX27 coimmunoprecipitation experiment with PTHR. HEK293 cells stably expressing HA-PTHR were treated with 100 nM PTH or vehicle for 5 min and then cross-linked by incubation in 2 mM DSP for 2 h on ice. The cross-linking reaction was terminated by the addition of 20 mM Tris (pH 7.5), and cells were lysed in RIPA buffer. HA-PTHR was immunoprecipitated using anti-HA-conjugated Sepharose beads. Endogenous SNX27 binding to the PTHR was determined by immunoblotting. *B*, quantitation of SNX27 binding normalized to untreated control shows that binding is enhanced by PTHR treatment ($p < 0.05$, $n = 3$). *C*, structural analysis of intact PDZ ligand requirement for PTHR binding to SNX27. HEK293 cells expressing Myc-SNX27 full-length protein and either wild-type HA-PTHR-ETVM or mutant HA-PTHR-ETVA were exposed to PTH for 5 min and then lysed and immunoprecipitated with anti-HA antibody. Myc-SNX27 coimmunoprecipitates with the receptor only when the PDZ ligand is intact. *D*, effect of PTH on localization of PTHR and SNX27. HEK293 cells transfected with GFP-tagged version of PTHR-ETVM, PTHR-ETVA, or PTHR-ΔKRK were treated for 5 min with 100 nM PTH or vehicle and then fixed in 3.6% paraformaldehyde and labeled with anti-SNX27 antibody. In unstimulated cells, wild-type PTHR is predominantly localized at plasma membranes, whereas SNX27 has a punctate intracellular distribution. Treatment with PTH promotes PTHR endocytosis and colocalization with SNX27. PTHR-ETVA internalized but with limited colocalization with SNX27. Mutation of the PTHR-ΔKRK ezrin-binding domain did not interfere with endocytosis or colocalization with SNX27. Images are representative of three independent experiments. *Scale bar*, 10 μm. *E*, compilation of quantitative colocalization of PTHR and SNX27 under control conditions ($n = 35$, 41, and 27 for -ETVA, -ETVM, and ΔKRK, respectively) or following PTH ($n = 47$, 48, and 41). **, $p < 0.01$ *versus* respective control. *Error bars*, S.E.

SNX27 either through its PDZ ligand or by virtue of its ezrin-binding motif. We hypothesized that PTHR binding to SNX27 occurs through PDZ domain interactions. Coimmunoprecipitation of SNX27 with PTHR stably expressed in HEK293 cells corroborated this theory. Under resting conditions, PTHR interaction with SNX27 was negligible (Fig. 2*A*). Treatment with 100 nM PTH promoted SNX27 binding to the wild-type receptor with an intact -ETVM PDZ motif (Fig. 2, *A* and *B*).

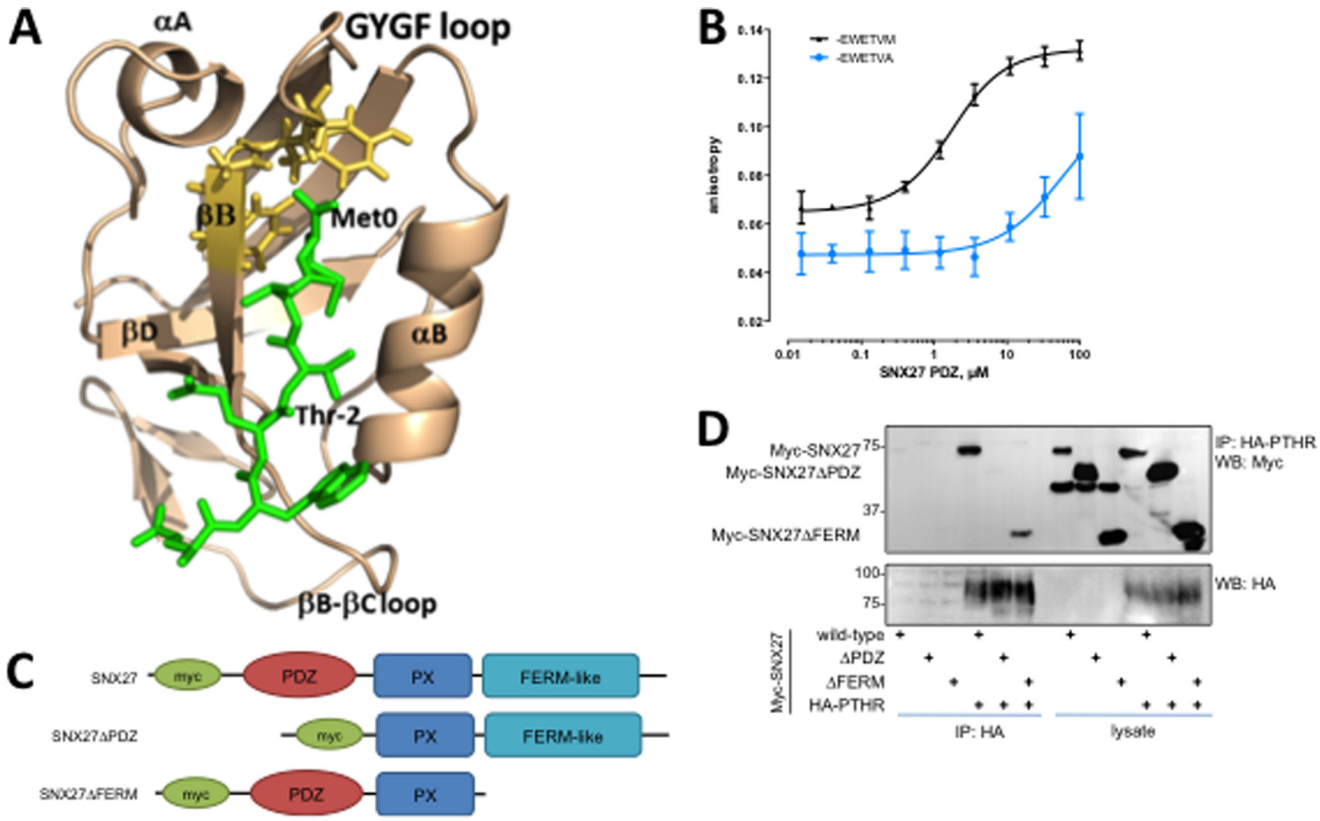

FIGURE 3. **Structural modeling and measurement of SNX27 binding to PTHR.** *A*, model structure of the SNX27 PDZ domain in complex with the C-terminal PTHR peptide. The PDZ domain and PTHR peptide are shown in *wheat* and *green*, respectively. The PTHR peptide (-EWETVM) is shown in a *stick representation* with residues numbered from 0 to −5. The GYGF loop of the PDZ domain is shown in *yellow* (*stick representation*). Residues forming the canonical hydrophobic pocket of PDZ are shown in *wheat* (*stick representation*). *B*, fluorescence anisotropy of SNX27 PDZ domain binding to PTHR. Representative binding curves for the FITC-labeled -EWETVM and -EWETVA peptides to the SNX27 PDZ domain are shown ($n = 3$). *C*, schematic representation of full-length Myc-tagged SNX27, PDZ deletion (*SNX27ΔPDZ*), and FERM deletion (*SNX27ΔFERM*) constructs used here. *D*, coimmunoprecipitation characterization of SNX27 structural determinants for PTHR binding. HEK293 and HA-PTHR stable cells were transiently transfected with the indicated Myc-SNX27 construct. Cells were treated with 100 nM PTH (5 min) and lysed in modified RIPA buffer. HA-PTHR was immunoprecipitated with anti-HA-conjugated Sepharose beads. The presence of bound SNX27 was detected by immunoblotting. Images are representative of $n = 3$ independent experiments. The results establish that PTHR binds to SNX27 by virtue of its PDZ domain. *Error bars*, S.E.

Replacement of the C-terminal Met with Ala (-ETVM), which disrupts PTHR interactions with the PDZ protein NHERF1 (74), abrogated PTH-induced interaction with SNX27 (Fig. 2*C*).

Having established that the PTHR binds SNX27 through its PDZ domain, we sought to identify the cellular sites of this interaction. Colocalization studies revealed that under basal conditions, PTHR is present mostly at the cell surface with little cytoplasmic expression and no colocalization with SNX27 (Fig. 2, *D* and *E*). Internal GFP-PTHR punctae noted under basal conditions may be constitutively internalized receptor or newly synthesized receptor in the biosynthetic pathway. After treatment with PTH for 5 min, PTHR localized to intracellular compartments that are positive for SNX27 (Pearson's correlation coefficient (r) = 0.60). Disrupting the PDZ ligand reduced colocalization (PTHR-ETVA $r = 0.36$). However, a PTHR mutant lacking the ezrin binding domain (ΔKRK) did not interfere with PTH-stimulated association of PTHR and SNX27 (ΔKRK $r = 0.61$). Thus, the colocalization findings are consistent with the coimmunoprecipitation results and confirm that an intact PDZ recognition motif is necessary and sufficient for binding of PTHR to SNX27.

The structural determinants of the interaction between PTHR and SNX27 were examined first by molecular dynamics simulation. The results show that the C-terminal motif of PTHR recognizes the SNX27 PDZ domain through canonical PDZ-ligand interactions (Fig. 3*A*). Primary contact occurs with the GYGF core-binding motif of the PDZ domain and the C-terminal Met at ligand position 0. We next characterized the binding affinity between the SNX27 PDZ domain and the PTHR by fluorescence anisotropy using purified recombinant SNX27 PDZ domain protein (residues 39–133) and a synthetic 6-residue PTHR C-tail peptide (PTHRct) labeled with FITC. The measured dissociation constant ($K_D = 1.2 \pm 0.1\ \mu$M) is consistent with a high specificity PDZ ligand recognition mechanism (Fig. 3*B*). Replacing the PTHRct terminal Met with Ala eliminated binding between the peptide and the SNX27 PDZ domain (Fig. 3*B*), consistent with the immunoprecipitation and colocalization studies. We then used well characterized SNX27 mutants (53) to define further the structural elements of the SNX27-PTHR interaction. HEK293 cells stably expressing HA-PTHR were transfected with wild-type SNX27 or with deletion mutants lacking either the PDZ (SNX27ΔPDZ) or FERM (SNX27ΔFERM) domains (Fig. 3*C*) (75). Wild-type SNX27 and SNX27ΔFERM interacted with the PTHR upon a 5-min exposure to PTH, whereas SNX27ΔPDZ did not bind PTHR (Fig. 3*D*),

indicating that the interaction with SNX27 proceeds through its PDZ domain. Thus, binding to SNX27 involves the PTHR PDZ ligand that interacts with the SNX27 PDZ domain.

SNX27 or VPS35 Knockdown Decreases the Rate of PTHR Recycling—If the ASRT complex mediates rapid PTHR recycling, then interfering with SNX27 or retromer should decrease receptor recycling. To test this idea, we first used a non-biased ELISA to measure the effect of SNX27 depletion on surface-delimited expression of the PTHR in a cell population (47). siRNA targeted to SNX27 delayed PTHR recycling at 20 min after ligand washout (Fig. 4*A*). To analyze the influence of SNX27 on PTHR recycling at the single cell level, we generated a PTHR tagged with SEP, a pH-sensitive GFP variant (76), in the N-terminal extracellular domain and established a stable HEK293 cell line expressing this receptor. We first validated that the SEP-PTHR signaled through cAMP comparable to the wild-type HA-PTHR (Fig. 4*B*). Confocal imaging of the SEP-PTHR shows that treatment with PTH induces internalization of the receptor followed by 80–90% fluorescence recovery within 60 min (Fig. 4*C*). We then applied time lapse TIRF microscopy to capture transient exocytic events at the cell surface of individual cells. The procedure is schematically illustrated in Fig. 4*D* (*top*). Upon agonist addition, internalization is induced, and receptors move to early endosomes, where the SEP tag is no longer fluorescent due to the acidity of the compartment. The receptor then recycles back to the surface, where it displays a burst of fluorescence. The *bottom panel* of Fig. 4*D* shows the lifetime of an illustrative individual exocytic event as it appears at the cell surface and then disperses across the plasma membrane. This method has been used previously and validated to study GPCR recycling (23, 70). We established that these exocytic events represent PTHR recycling and not *de novo* receptor biogenesis by inhibiting new protein synthesis with cycloheximide. Vehicle-treated cells exhibited a low rate of basal exocytosis (1.4 ± 0.3 events/10 μm^2 min^{-1}) that increased significantly upon incubation with 100 nM PTH (16.7 ± 1.4 exocytic events/10 μm^2 min^{-1}; $p < 0.001$) and was unaffected by pretreatment with 10 μM cycloheximide (16.9 ± 1.4 exocytic events/10 μm^2 min^{-1}) (Fig. 4*E* and supplemental Videos 1 and 2).

Knockdown with two distinct shRNAs each reduced SNX27 expression by 40% (Fig. 4*F*). When cotransfected together, exocytosis decreased by 50% in knockdown cells (9.9 ± 1.1/10 μm^2 min^{-1}) compared with control cells expressing scrambled shRNA (19.4 ± 2.2/10 μm^2 min^{-1}; $p < 0.01$) after a 5-min incubation with 100 nM PTH (Fig. 4*G* and supplemental Video 3). This effect was specific for SNX27 and not due to off-target shRNA effects insofar as recycling was rescued by co-expression of shRNA-resistant SNX27 but not by a mutant lacking the PDZ domain (Fig. 4*F*; Myc-SNX27 = 17.07 ± 3.5/10 μm^2 min^{-1} *versus* Myc-SNX27ΔPDZ = 7.28 ± 1.2/10 μm^2 min^{-1}).

SNX27 is a cargo selector for receptor trafficking through the retromer complex (4, 16), and the PTHR interacts with retromer in early endosomes (42). This suggests that retromer VPS subunits should be present with the PTHR in endosomes. Mass spectrometry of endosome purified after PTH stimulation revealed the presence of VPS26, VPS29, and VPS35 peptide fragments (Table 1).

According to this paradigm, disrupting the retromer complex should interfere with PTHR recycling much as SNX27 does. To verify the supposition that rapid SNX27-dependent PTHR recycling is mediated by retromer, we knocked down expression of VPS35 (Fig. 5*A*), one of the retromer protomers, and measured the rate of exocytosis after PTHR activation. Upon VPS35 depletion, retromer function was suppressed, and the rate of exocytosis significantly decreased from 14.1 ± 2.5 to 3.8 ± 0.4 exocytic events/10 μm^2 min^{-1} ($p < 0.01$) (Fig. 5*B* and supplemental Video 4).

The retromer complex is associated with the actin nucleation activator WASH complex, which controls actin dynamics to transport cargo vesicles to the cell surface (11, 12). This model predicts that rapid recycling of PTHR by SNX27 and retromer requires an intact filamentous actin network. To determine whether rapid PTHR recycling depends on actin, we used LatA, an actin-depolymerizing agent, and measured the rate of exocytosis after PTH treatment. LatA significantly decreased the rate of PTHR exocytosis following the addition of PTH (Fig. 5*C* ($p < 0.0001$) and supplemental Videos 5 and 6), a 50% reduction when compared with vehicle-treated cells (Fig. 5*D*; $p < 0.005$). Thus, rapid PTHR recycling requires all three ASRT components: actin, SNX27, and retromer.

To confirm that SNX27 depletion specifically affects recycling of receptors possessing a PDZ ligand, we performed control experiments that analyzed the effect of SNX27 knockdown on recycling of the transferrin receptor, a transmembrane carrier protein lacking a PDZ ligand that rapidly and constitutively recycles to the plasma membrane independent of ligand binding (77). Knockdown of SNX27 or VPS35 did not measurably affect trafficking of the SEP-transferrin receptor (Fig. 5*E*; 23.4 ± 3.6 exocytic events/10 μm^2 min^{-1} (scrambled) *versus* 18.41 ± 1.8 exocytic events/10 μm^2 min^{-1} (shSNX27) and 21.24 ± 3.9 exocytic events/10 μm^2 min^{-1} (shVPS35)). These findings establish the PDZ ligand specificity of SNX27- and retromer-dependent GPCR recycling.

SNX27-independent PTHR Recycling—Although PTHR binding to SNX27 relies upon the PTHR PDZ ligand interaction and SNX27 depletion reduces the rate of PTHR recycling, the results do not exclude the possibility that PTHR recycling also may occur autonomously. To test this possibility, we generated a SEP-PTHR, wherein the C-terminal Met was mutated to Ala (SEP-PTHR-ETVA). PTHR-ETVA with a disrupted PDZ ligand recycled at a rate and to an extent similar in both whole cell recycling (Fig. 6*A*) and TIRF single event exocytosis assays (Fig. 6*B*) to that of PTHR-ETVM with an intact PDZ ligand. To reconcile these findings, we hypothesized that PTHR-ETVA interacts with the retromer complex independent of SNX27. We first determined whether the PTHR-ETVA mutant maintained trafficking to the retromer complex following PTH treatment by coimmunoprecipitating the PDZ ligand-intact PTHR-ETVM and the mutant PTHR-ETVA receptor after 5- and 15-min incubations with PTH. SNX27 and VPS35 were enriched with the full-length receptor after 5 min of PTH treatment and were less abundant at 15 min. In contrast, PTHR-ETVA did not bind SNX27, and VPS35 was immunoprecipi-

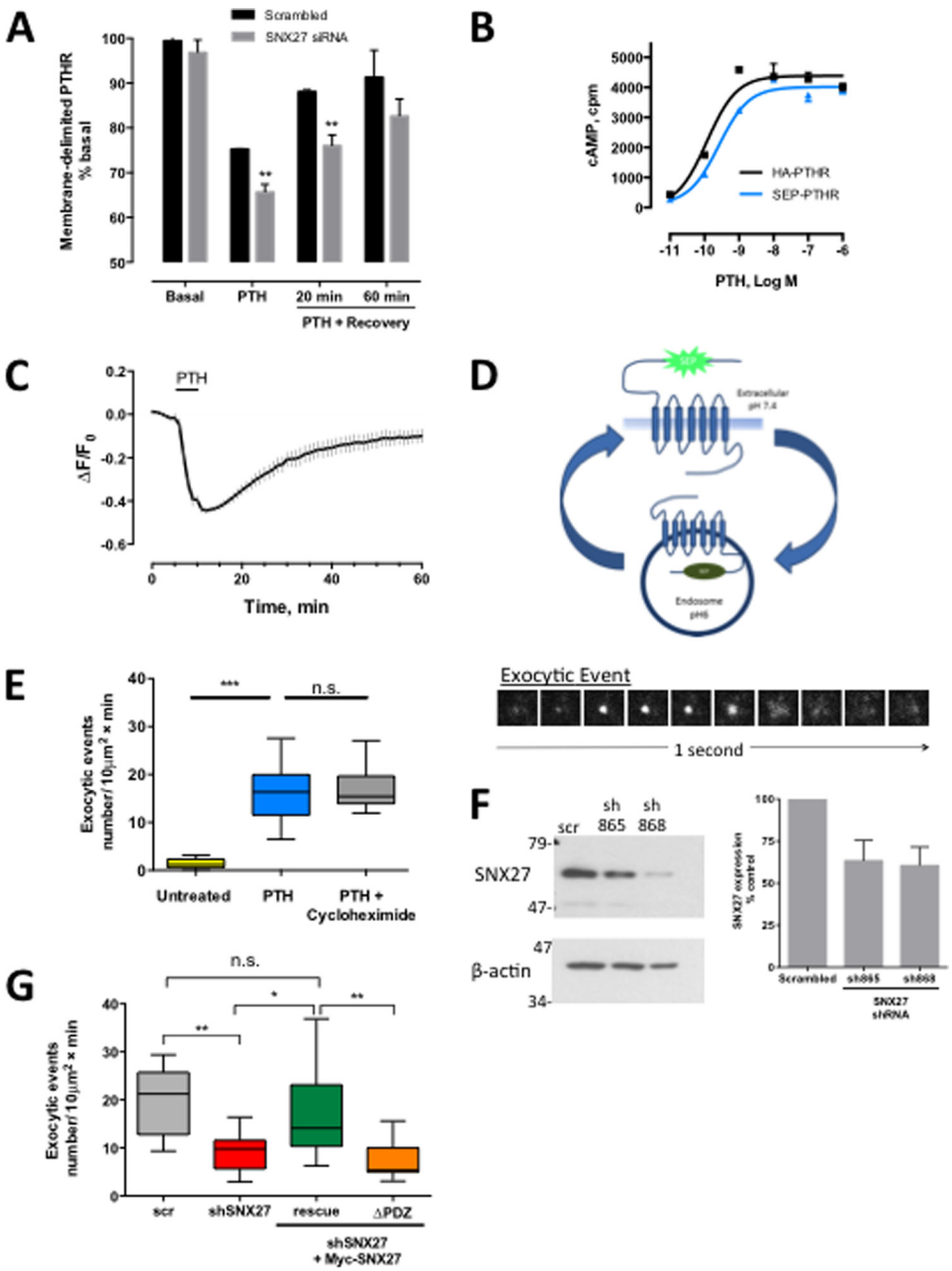

FIGURE 4. **SNX27 depletion reduces PTHR recycling.** *A*, ELISA of PTHR recycling. HEK293 cells stably expressing the HA-PTHR were transfected with scrambled or SNX27 siRNA. PTH was added as shown, and the cells were allowed to recover for the indicated time. SNX27 depletion resulted in reduced recovery of surface PTHR. $n = 3$; **, $p < 0.01$ *versus* respective control. *B*, SEP-PTHR activity was compared with HA-PTHR by cyclic AMP accumulation. SEP-PTHR activated cAMP production at a rate indistinguishable from HA-PTHR. *C*, time lapse confocal microscopy analysis of PTHR recycling. SEP-PTHR recycling was measured after agonist-induced internalization. Images were acquired at 1-min intervals. After a baseline was established, cells were treated with 100 nM PTH for 5 min and then washed out. SEP-PTHR surface expression recovered to 80% of initial levels within 50 min of agonist removal ($n = 6$). *D*, TIRF-based measurement of PTHR exocytosis. The *top panel* illustrates the principle of SEP-tagged PTHR to capture transient exocytic events at the surface of individual cells. Upon receptor internalization, the SEP tag is no longer fluorescent due to the acidity of the endosomal compartment. When the receptor recycles to the surface, it displays a fluorescent burst. This is shown in the *bottom panel*, where exocytic events are seen at the cell surface as transient clusters of fluorescence appearing and dispersing after 1–2 s. The number of exocytic events/min were counted and normalized to the area of the cell. *E*, stimulation of single PTHR exocytic events by PTH. Under basal conditions, the rate of spontaneous exocytosis is low; the addition of 100 nM PTH causes a >10-fold increase in the rate of exocytosis (vehicle, 1.4 ± 0.4 exocytic events/10 μm^2 min^{-1}; PTH, 16.7 ± 1.4 exocytic events/10 μm^2 min^{-1}; $n = 8–22$, $p < 0.01$). 2-h pretreatment with 10 μM cycloheximide to prevent *de novo* protein synthesis did not affect the rate of receptor exocytosis (PTH, 16.7 ± 1.4 exocytic events/10 μm^2 min^{-1}; PTH with cycloheximide, 16.9 ± 1.3 exocytic events/10 μm^2 min^{-1}). *F*, effect of shRNA on SNX27 expression. HEK293 cells were transiently transfected with two shRNAs targeted to SNX27. Cell lysates were prepared 72 h after transfection, and SNX27 protein expression was analyzed by immunoblotting. Both shRNAs reduced protein expression by 50%. β-Actin was used as a loading control. *G*, effect of shRNA against SNX27 on single PTHR exocytic events. SEP-PTHR HEK293 cells were transiently transfected with scrambled (*scr*) shRNA or cotransfected with shSNX27 (*shSNX27 865* + *shSNX27 868*) for 72 h. Exocytosis was measured by time lapse TIRF microscopy as detailed under "Experimental Procedures." SNX27 knockdown decreased the rate of exocytosis by 50% at 5 min after the addition of PTH ($n = 14–16$, $p < 0.01$). This inhibitory effect was rescued by expression of a rescue shRNA-resistant SNX27 construct but not with a mutant lacking the PDZ domain. *Error bars*, S.E.

TABLE 1

Mass spectrometry identification of endosomal VPS peptides isolated with PTHR

Gene symbol, peptide sequence, observed theoretical *m/z*, charge state, cross-correction, accession number, and sequence coverage are listed. The downward arrows following the first residue and preceding the last indicate the sites of trypsin cleavage. Differences in protein coverage for VPS proteins may be due to 1) variable retention during isolation, 2) dissimilar trypsinization properties of the three VPS subunits, and 3) distinct ionization properties of VPS tryptic peptides during MS analysis with fragments outside the detection range (90). Obs *m/z*, observed theoretical *m/z*; *z*, charge state; Xcorr, cross-correction.

Gene symbol	Peptide	Obs *m/z*	*z*	ppm	XCorr	Accession no.	Sequence coverage
							%
VPS26A	R ↓ YFLNLVLVDEEDRR ↓ Y	594.31249	3	0.03	2.863	O75436	4.3
VPS29	K ↓ IGLIHGHQVIPWGDMASLALLQR ↓ Q	842.46618	3	1.24	4.115	Q9UBQ0-1	32.4
	R ↓ GDFDENLNYPEQK ↓ V	784.84689	2	0.07	3.329		
	R ↓ QFDVDILISGHTHKFEAFEHENK ↓ F	686.08939	4	1.44	3.077		
VPS35	K ↓ HFHPLFEYFDYESR ↓ K	629.62145	3	0.1	3.942	Q96QK1	12.7
	R ↓ KVADLYELVQYAGNIIPR ↓ L	688.04981	3	0.88	3.756		
	K ↓ VADLYELVQYAGNIIPR ↓ L	645.35091	3	−0.02	3.233		
	R ↓ ACAELHQNVNVK ↓ N	461.56638	3	0.11	3.083		
	K ↓ AQLAAITLIIGTFER ↓ M	539.65083	3	0.58	2.972		
	R ↓ LSQLEGVNVER ↓ Y	622.33586	2	0.31	2.969		
	R ↓ FTLPPLVFAAYQLAFR ↓ Y	618.68235	3	0.67	2.829		
	K ↓ LFDIFSQQVATVIQSR ↓ Q	618.00391	3	0.45	2.335		

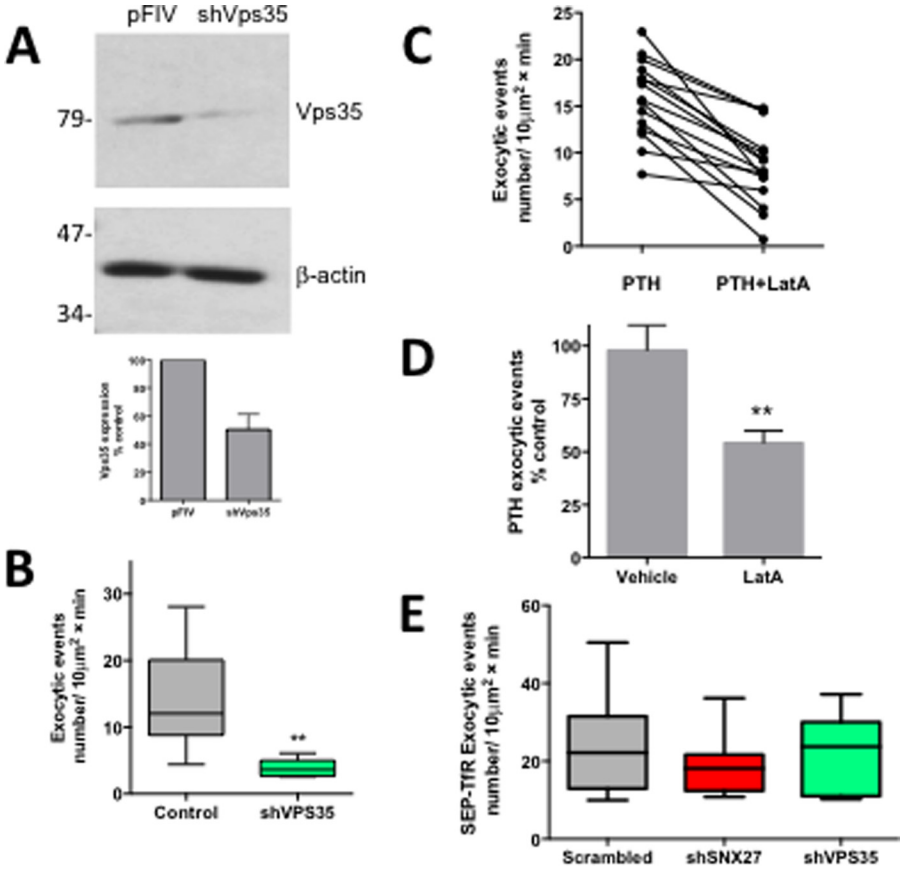

FIGURE 5. **Depletion of VPS35 or actin inhibition reduces PTHR exocytosis.** *A*, shRNA depletion of VPS35. HEK293 cells were transiently transfected with pFIV-mCherry control vector or pFIV-mCherry-shVPS35. Cell lysates were prepared 72 h post-transfection, and VPS35 protein expression was analyzed by immunoblotting. VPS35 was efficiently depleted by shRNA. β-Actin was used as a loading control. *B*, SEP-PTHR HEK293 cells were transiently transfected with pFIV-mCherry or pFIV-sh VPS35-mCherry for 72 h. Exocytosis was measured by time lapse TIRF microscopy. Activity-dependent recycling of the PTHR is reduced by >70% when VPS35 is depleted by shRNA knockdown (pFIV-mCherry, 14.1 ± 2.5 exocytic events/10 μm^2 min^{-1}; sh VPS35, 3.8 ± 0.4 exocytic events/10 μm^2 min^{-1}; $p < 0.01$). *C*, SEP-PTHR cells were treated with 100 nM PTH. After 5 min, surface fluorescence was bleached with high laser power, and a time lapse TIRF video was acquired. After image acquisition, 10 mM latrunculin A was added for a further 5 min, and a second time lapse video was acquired. LatA significantly decreased the rate of exocytosis following PTH treatment (PTH, 15.76 ± 1.1 exocytic events; LatA, 8.5 ± 1.1 exocytic events; paired *t* test, $p < 0.0001$). *D*, LatA caused a 50% reduction in recycling when compared with vehicle-treated cells (unpaired *t* test, $p < 0.005$). *E*, SEP-transferrin receptor trafficking was not affected by SNX27 or VPS35 knockdown. Data represent mean ± S.E. (*error bars*) ($n = 7$–14).

tated but less so compared with wild-type receptor (Fig. 6*C*). These findings imply that PTHR binds retromer independent of its PDZ ligand. To test this, we performed overlay assays, where recombinant VPS26, VPS29, and VPS35 protein were individually immobilized on a PVDF membrane and incubated with purified PTHR-ETVM or PTHR-ETVA. Both the wild-type PDZ ligand intact PTHR-ETVM receptor and the PTHR-ETVA mutant bound robustly to VPS26 but not VPS29 or VPS35 (Fig. 6*D*). We next inquired whether VPS26 might assemble a ternary complex with PTHR and SNX27. According

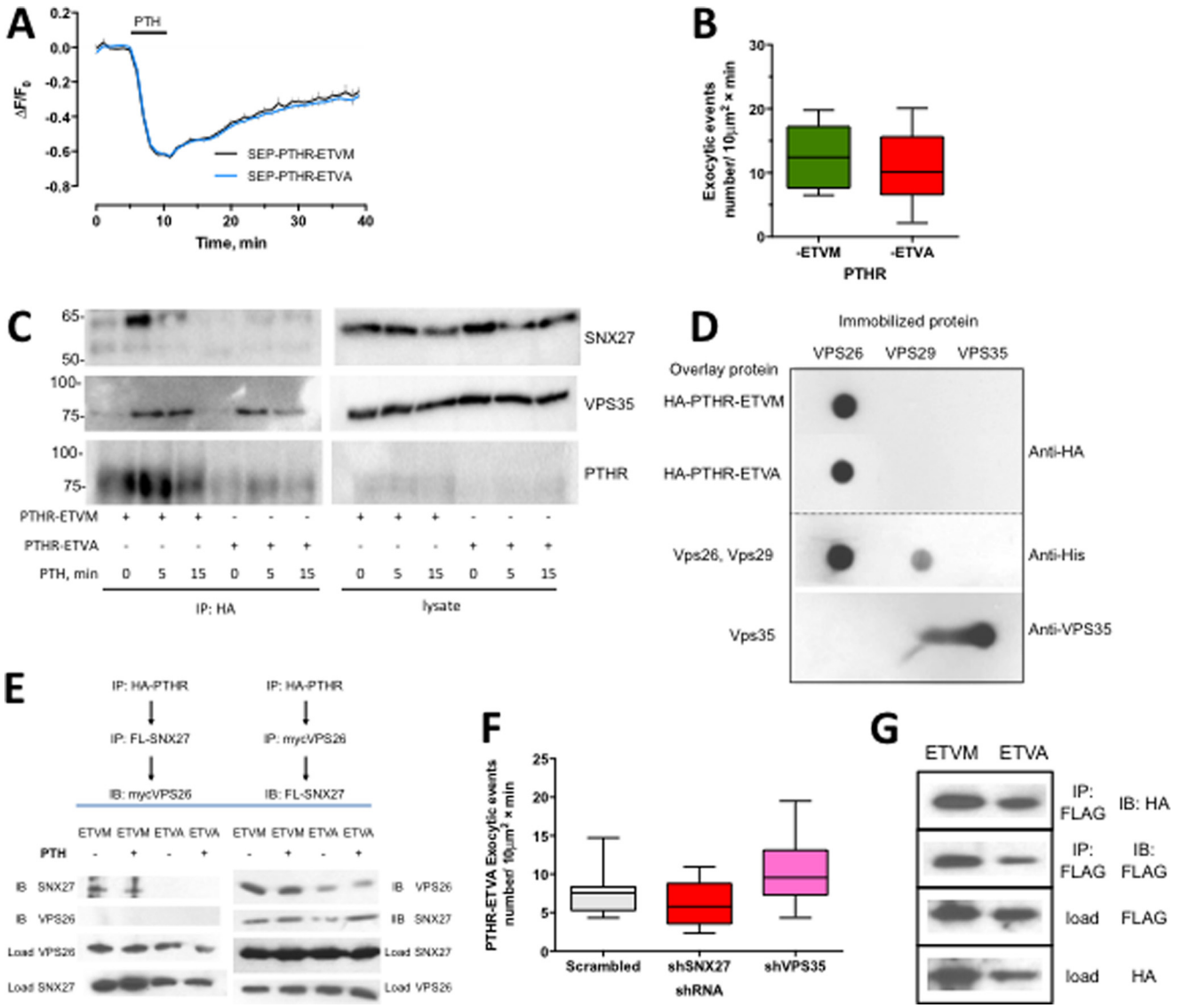

FIGURE 6. **PDZ ligand autonomous PTHR-retromer interaction and recycling.** *A*, whole cell recycling of PTHR with intact or disrupted PDZ ligand measured by time lapse confocal microscopy. Recycling of either intact SEP-PTHR-ETVM (*black*) or mutant SEP-PTHR-ETVA (*blue*) was measured following PTH-induced receptor internalization. After a 5-min baseline was established, cells were treated with 100 nM PTH for 5 min and then washed out ($n = 10$, ETVM, ETVA). *B*, single exocytic events were measured by time lapse TIRF microscopy as before. At 5 min after the addition of 100 nM PTH, the rate of exocytosis was indistinguishable between PTHR-ETVM (12.8 ± 1.9 exocytic events) and PTHR-ETVA (11.3 ± 1.7 exocytic events) ($p = 0.62$). *C*, coimmunoprecipitation analysis of PTHR-ETVM and PTHR-ETVA binding to SNX27 and VPS35. GnTI HEK293 cells stably expressing HA-PTHR-ETVM or HA-PTHR-ETVA were treated with 100 nM PTH for 5 or 15 min and then cross-linked by incubation in DSP for 2 h on ice. The cross-linking reaction was terminated by the addition of 20 mM Tris (pH 7.5), and the cells were lysed in RIPA buffer. HA-PTHR was immunoprecipitated using anti-HA-conjugated Sepharose beads, and the presence of SNX27 and VPS35 in complex with the receptor was determined by immunoblotting. SNX27 and VPS35 were present in abundance after a 5-min PTH treatment of HA-PTHR-ETVM cells and at a lesser degree after 15 min. SNX27 did not coimmunoprecipitate with PTHR-ETVA, but binding to retromer could be detected at both 5 and 15 min after PTH treatment. *D*, overlay analysis of PTHR-ETVA and PTHR-ETVA interactions with purified VPS protomers. VPS26, VPS29, and VPS35 protein were applied to Immobilon P membranes under vacuum. 10 μg of HA-PTHR-ETVA or HA-PTHR-ETVA protein, as indicated, was overlaid. HA-PTHR bound to the retromer components was detected with a polyclonal anti-HA antibody. The presence of immobilized His-VPS26 and His-VPS29 was confirmed with a monoclonal anti-His antibody; immobilized VPS35 was established with a polyclonal anti-VPS35 antibody. Images are representative of three independent experiments. *E*, sequential assembly of a PTHR-VPS26-SNX27 protein complex. The *top panel* shows the sequence in which the serial immunoprecipitation was performed, and the *bottom panel* shows the respective results. The PTHR forms a ternary complex only when it first interacts in VPS26. The results are illustrative of four independent experiments. *F*, comparison of SNX27 and VPS35 down-regulation on PTHR-ETVA recycling. HEK293 cells stably expressing SEP-PTHR-ETVA were transiently transfected for 72 h with shRNA against SNX27 or VPS35. Exocytosis was measured by time lapse TIRF microscopy. Activity-dependent recycling of the PTHR was not altered by shRNA knockdown of VPS35 or SNX27 compared with control shRNA (scrambled shRNA, 7.6 ± 0.8 ($n = 11$); shSNX27, 6.123 ± 0.8 ($n = 11$); shVPS35, 10.1 ± 1.0 ($n = 15$) exocytic events). *G*, NSF binding to PTHR-ETVM and PTHR-ETVA. CHO cells were transfected with FLAG-PTHR-ETVM or -ETVA, as indicated, and HA-NSF. PTHR was immunoprecipitated with FLAG-M2 affinity gel. PTHR and NSF were detected by immunoblotting using anti-FLAG and anti-HA antibodies, respectively, as described under "Experimental Procedures." Similar results were obtained in four independent experiments. *Error bars*, S.E.

to this idea, VPS26 could bind both wild-type PTHR-ETVM and the PTHR-ETVA PDZ mutant and in turn bind SNX27. However, only the PTHR-ETVM could assemble a complex with SNX27 and VPS26. We tested this idea by performing sequential coimmunoprecipitation experiments. The results shown in Fig. 6*E* support the view that an ordered assembly of the ternary complex proceeds when the PTHR first engages VPS26, which then interacts with SNX27. To determine

whether recycling of the PTHR-ETVA mutant requires the ASRT complex, we depleted SNX27 or VPS35 and found that the rate of PTHR-ETVA exocytosis was not significantly different when components of the ASRT were absent (Fig. 6*F*). Thus, PTHR-ETVA binds retromer and SNX27, but receptor recycling is independent of ASRT.

NSF is a vesicle-fusing ATPase that participates in trafficking and surface expression of several transmembrane receptors (78–80). NSF binds target proteins that possess a C-terminal (D/E)(S/T)(L/V)*X* sequence (78, 81). As such, NSF should bind both PTHR forms, unlike the SNX27 PDZ-binding motif that recognizes PTHR-ETVM but not PTHR-ETVA. We analyzed PTHR binding to NSF by coimmunoprecipitation assays in CHO cells because they do not express NHERF1, another PDZ protein that might confound results. The results illustrated in Fig. 6*G* show robust interaction of PTHR-ETVM and PTHR-ETVA with NSF, consistent with the structural requirements of the NSF binding motif.

Discussion

The PTHR is a class B GPCR that exhibits a long recycling time compared with class A receptors. Complete PTHR recycling occurs within 1–2 h after removal of the ligand and coincides with but does not require receptor dephosphorylation (33, 34, 44, 82). Here, we demonstrate that the PTHR is a novel cargo for rapid receptor recycling through the ASRT complex, facilitating the surface recycling of some internalized receptor within minutes after ligand binding. Direct endosome-to-plasma membrane recycling has not previously been considered for the PTHR, which traffics to the Golgi compartment after prolonged (30-min) treatment with PTH, in a phospholipase D-dependent manner (83). Because SNX27 has been linked to the fast recycling of other GPCRs harboring a PDZ ligand, we theorized that a similar mechanism mediates rapid PTHR recycling.

Endogenous SNX27 interacts with the receptor after PTH stimulation and colocalizes in endosomal EEA1-positive intracellular organelles. The SNX27 PDZ domain shares the same GYGF core-binding motif as NHERF1, another PTHR-interacting protein; therefore, PDZ interactions were most likely to account for binding. However, SNX27 also contains a FERM-like domain, and PTHR has been shown to bind the FERM domain of ezrin, which requires the KRK motif in the C terminus of the receptor (72). The SNX27 FERM domain recognizes proteins with an NP*X*Y motif (15), which is not present in the PTHR C terminus (73). To assess the structural determinants of this interaction, we used theoretical modeling and experimental approaches. Molecular modeling revealed that the PDZ ligand of the receptor could engage the SNX27 PDZ domain in a manner similar to its interaction with NHERF1. A deletion mutant of SNX27 lacking a PDZ domain and PTHR harboring a mutated PDZ ligand showed that either disrupts binding of these proteins. Consistent with the view that the SNX27 PDZ domain mediates PTHR binding, deletion of the SNX27 FERM domain did not affect binding to the PTHR.

Various routes exist to recycle transmembrane receptors, and receptors can follow more than one itinerary to the plasma membrane (84). SNX27 mediates fast recycling of several transmembrane receptors that possess a C-terminal PDZ ligand, as does the PTHR (4, 18–20). To investigate rapid recycling of the PTHR, we used a TIRF assay to measure rapid, single exocytic events at the surface of individual cells. The SEP tag is fluorescent at neutral pH, when the protein is at the cell surface, but not at the acidic pH found in early endosomes (76). The advantage of this technique is that it allows visualization of early and discrete exocytic events that would not be discernable or captured by whole-cell fluorescence measurements. A limitation of the present study is that the TIRF assay does not provide quantitative information on the number of receptors being delivered to the cell surface and relies on heterologous cells that overexpress the receptor. Additionally, the rate and extent of exocytic events in cells are variable. We controlled for this by normalizing to the visible TIRF area. Within these parameters, PTHR recycling was no more variable than reported for other GPCRs (22, 23, 70). This single event assay also necessitates the overexpression of a fluorescently tagged receptor that might result in elevated receptor recycling compared with cells expressing endogenous levels of the receptor. To compensate for some of these potential liabilities, we applied an unbiased, population-based ELISA of constitutive PTHR recycling. Both results point to a central role of SNX27 and to the capacity of PTHR to recycle rapidly. It should be pointed out that although PTHR is overexpressed, experiments were performed at constitutive internalization/recycling protein levels.

The employed shRNA expresses mCherry. This permits estimating that 50–60% of the cells were transfected and allowed us to select cells expressing the shRNA knockdown construct during the TIRF assay, in which we measure PTHR recycling in single cells. shRNA depletion of SNX27 expression reduced PTHR recycling by 50%. Down-regulating SNX27 did not abolish PTHR recycling. Incomplete inhibition of PTHR recycling presumably results from a combination of partial protein knockdown, direct interaction between the PTHR and retromer, recycling through a different pathway, or use of an alternate trafficking chaperone. Insofar as the reduction of recycling observed with retromer depletion or upon actin inhibition is similar to that achieved with SNX27 depletion, we interpret these findings to indicate a primary but not exclusive role of the ASRT complex in mediating rapid PTHR recycling. However, the findings do not exclude the possibility that the PTHR can be routed to the cell surface by bulk membrane recycling or in association with other chaperone adaptor proteins.

Although we showed that PTHR interacts with retromer (41, 42), the structural determinants of this interaction were undefined. The VPS26 subunit has an arrestin-like fold that enables binding of transmembrane receptors (54). The VPS35 subunit can bind the cytoplasmic tail of transmembrane receptors, such as the mannose phosphate receptor, where binding is thought to involve an α-solenoid fold (8, 85). Thus, PTHR might interact with either or both VPS26 and VPS35 retromer subunits. The present study establishes that this interaction occurs through the VPS26 subunit, which directly binds the PTHR. Such binding does not involve particular structural motifs, such as PDZ recognition sequences, because both PDZ-intact and disrupted forms of the PTHR bound VPS26. Hence, an interaction with both wild type and PTHR-ETVA is consistent. More-

over, this finding also rules out the KRK-ezrin binding domain as mediating the interaction between PTHR and retromer. We did not find direct binding of VPS35 either to the wild-type receptor or to the PTHR-ETVA mutant. The immunoprecipitation studies disclose a distinct reaction order for the assembly of the PTHR-retromer-SNX27 ternary complex. Thus, PTHR first engages VPS26 and then SNX27, which directly binds to the retromer complex (16). Formation of the ternary complex failed when trying to assemble PTHR first with SNX27 and then VPS26.

Mutating the PDZ ligand reduced the affinity of PTHR for retromer but unexpectedly did not affect the rate at which receptors are returned to the cell surface. Several possibilities may account for this unanticipated behavior. Previous studies of PTHR recycling used C-terminal GFP-tagged constructs that may have occluded PDZ interactions but which recycled over 1–2 h (34, 44). This suggested that PDZ-defective receptors may traffic through a different route, possibly by virtue of posttranslational modifications, such as phosphorylation or ubiquitination (86), or interactions that would normally be obstructed by PDZ protein binding. Mutations within the C-terminal tail of other receptors that affect phosphorylation sites can result in differences of protein trafficking (22, 23, 70).

NSF may offer an alternate mechanism to PDZ-dependent sorting but one that still involves the C-terminal PTHR sequence. NSF is a vesicle-fusing ATPase that binds SNARE complexes to separate them during ATP hydrolysis and disassembly of the SNARE complex (87). The PDZ-binding motif takes the form -(D/E)(S/T)$X\varphi$, where X is promiscuous and φ is a hydrophobic residue. NSF recognizes the sequence -(D/E)(S/T)(L/V)X (78, 81). Thus, the two motifs are largely synonymous except for the location of the permissive residue. NSF affects trafficking and surface expression of several transmembrane receptors (78–80). The β_2AR, for instance, is excluded from retromer tubules when the PDZ ligand is occluded (4), and its recycling also is regulated by NSF (78). Eliminating PDZ interactions of PTHR reduced binding to the retromer complex subunits but did not abolish recycling. To summarize, 1) the SNX27 PDZ domain binds the PTHR C terminus. 2) The presence of the PTHR-ETVM motif promotes colocalization of PTHR and SNX27 in endosomes. 3) Knocking down SNX27 retards rapid PTHR recycling. 4) The PDZ domain of SNX27 is required to rescue the effect of SNK27 knockdown on rapid PTHR recycling. 5) PTHR-ETVA, which does not bind SNX27, recycles at the same rate as PTHR-ETVM. Binding of the PTHR-ETVM motif to the SNX27 PDZ domain is involved in but not required for PTHR recycling. Thus, SNX27 contributes to rapid PTHR recycling. 6) PTHR can undergo SNX27-independent recycling either through ordered assembly of a complex with retromer and direct engagement of retromer with SNX27 or through an independent recycling mechanism involving NSF.

We interpret these findings to mean that PTHR can recycle rapidly via at least two pathways, one involving the ASRT complex and using the ETVM-SNX27 PDZ domain interaction. The ASRT complex through its individual actin, SNX27, and retromer elements promotes a rapid recycling component of PTHR and reveals a novel aspect of endosomal receptor sorting. The finding that knockdown of SNX27 partially inhibited rapid recycling supports the idea of an alternative rapid recycling pathway independent of the ASRT complex and possibly involving NSF. Insofar as the PTHR-ETVM and PTHR-ETVA recycle at the same rate, we speculate that the PTHR can engage either recycling pathway with similar functional efficiency. Finally, because the experiments were of necessity performed with PTHR overexpression, we cannot conclude with certainty whether ASRT or ASRT-independent recycling predominates under physiological conditions.

While the present study was under review, a complementary investigation reported compatible findings that additionally demonstrate an important role of SNX27 on PTH actions on skeletal development (88). Global SNX27 knock-out decreased multiple parameters of bone architecture in post-natal mice. These studies further confirm the present observations that PTHR associates with the binding pocket of the SNX27-PDZ domain. A second related study demonstrated that FAM21 (family with sequence similarity-21) interacts with SNX27, thereby restricting SNX27 within endosomal subcompartments and preventing cargoes from being transported to the Golgi apparatus (89).

Author Contributions—P. A. F. and J. C. M. designed the study and wrote the paper. K. X., F. J. A., and J. P. V. developed the endosomal mass spectrometry protocol and acquired and analyzed mass spectrometry data. A. B. and Q. Z. synthesized peptides and purified proteins. T. M. performed computational modeling and fluorescence polarization and analyzed data. J. C. M., S. L. B., and M. A. P. designed, performed, and analyzed TIRF experiments. J. A. A. conducted ELISAs of PTHR endocytosis. J. C. M. and W. B. S. performed biochemical studies and molecular cloning. All authors reviewed the results and approved the final version of the paper.

Acknowledgments—Myc-tagged SNX27 constructs were a kind gift from Dr. Martin Playford (National Institutes of Health). Dr. Kevin Wilkinson (University of Bristol) generously provided shVPS35-mCherry. Dr. Mark von Zastrow (University of California, San Francisco, CA) supplied plasmids for SNX27 PDZ(39–133). Cp-VPS29 was a gift from Dr. Cheryl Arrowsmith (University of Toronto), His-VPS35 was contributed by Dr. Brett Collins (University of Queensland), and pmr101A-hVPS26 was contributed by Dr. James Hurley (University of California, Berkeley, CA). Dr. Alexandre Gidon performed the pH measurements. Dr. Nathan Pavlos graciously shared results prior to publication.

References

1. Ferguson, S. S. (2001) Evolving concepts in G protein-coupled receptor endocytosis: the role in receptor desensitization and signaling. *Pharmacol. Rev.* **53,** 1–24
2. Hanyaloglu, A. C., and von Zastrow, M. (2008) Regulation of GPCRs by endocytic membrane trafficking and its potential implications. *Annu. Rev. Pharmacol. Toxicol.* **48,** 537–568
3. Tsvetanova, N. G., Irannejad, R., and von Zastrow, M. (2015) G protein-coupled receptor (GPCR) signaling via heterotrimeric G proteins from endosomes. *J. Biol. Chem.* **290,** 6689–6696
4. Temkin, P., Lauffer, B., Jäger, S., Cimermancic, P., Krogan, N. J., and von Zastrow, M. (2011) SNX27 mediates retromer tubule entry and endosome-to-plasma membrane trafficking of signalling receptors. *Nat. Cell Biol.* **13,** 715–721
5. Harbour, M. E., Breusegem, S. Y., Antrobus, R., Freeman, C., Reid, E., and

Seaman, M. N. (2010) The cargo-selective retromer complex is a recruiting hub for protein complexes that regulate endosomal tubule dynamics. *J. Cell Sci.* **123,** 3703–3717
6. Wassmer, T., Attar, N., Harterink, M., van Weering, J. R., Traer, C. J., Oakley, J., Goud, B., Stephens, D. J., Verkade, P., Korswagen, H. C., and Cullen, P. J. (2009) The retromer coat complex coordinates endosomal sorting and dynein-mediated transport, with carrier recognition by the *trans*-Golgi network. *Dev. Cell* **17,** 110–122
7. Haft, C. R., de la Luz Sierra, M., Bafford, R., Lesniak, M. A., Barr, V. A., and Taylor, S. I. (2000) Human orthologs of yeast vacuolar protein sorting proteins Vps26, 29, and 35: assembly into multimeric complexes. *Mol. Biol. Cell* **11,** 4105–4116
8. Hierro, A., Rojas, A. L., Rojas, R., Murthy, N., Effantin, G., Kajava, A. V., Steven, A. C., Bonifacino, J. S., and Hurley, J. H. (2007) Functional architecture of the retromer cargo-recognition complex. *Nature* **449,** 1063–1067
9. Rojas, R., Kametaka, S., Haft, C. R., and Bonifacino, J. S. (2007) Interchangeable but essential functions of SNX1 and SNX2 in the association of retromer with endosomes and the trafficking of mannose 6-phosphate receptors. *Mol. Cell. Biol.* **27,** 1112–1124
10. Linardopoulou, E. V., Parghi, S. S., Friedman, C., Osborn, G. E., Parkhurst, S. M., and Trask, B. J. (2007) Human subtelomeric WASH genes encode a new subclass of the WASP family. *PLoS Genet.* **3,** e237
11. Derivery, E., Sousa, C., Gautier, J. J., Lombard, B., Loew, D., and Gautreau, A. (2009) The Arp2/3 activator WASH controls the fission of endosomes through a large multiprotein complex. *Dev. Cell* **17,** 712–723
12. Gomez, T. S., and Billadeau, D. D. (2009) A FAM21-containing WASH complex regulates retromer-dependent sorting. *Dev. Cell* **17,** 699–711
13. Helfer, E., Harbour, M. E., Henriot, V., Lakisic, G., Sousa-Blin, C., Volceanov, L., Seaman, M. N., and Gautreau, A. (2013) Endosomal recruitment of the WASH complex: active sequences and mutations impairing interaction with the retromer. *Biol. Cell* **105,** 191–207
14. van Weering, J. R., and Cullen, P. J. (2014) Membrane-associated cargo recycling by tubule-based endosomal sorting. *Semin. Cell Dev. Biol.* **31,** 40–47
15. Ghai, R., Bugarcic, A., Liu, H., Norwood, S. J., Skeldal, S., Coulson, E. J., Li, S. S., Teasdale, R. D., and Collins, B. M. (2013) Structural basis for endosomal trafficking of diverse transmembrane cargos by PX-FERM proteins. *Proc. Natl. Acad. Sci. U.S.A.* **110,** E643–652
16. Steinberg, F., Gallon, M., Winfield, M., Thomas, E. C., Bell, A. J., Heesom, K. J., Tavaré, J. M., and Cullen, P. J. (2013) A global analysis of SNX27-retromer assembly and cargo specificity reveals a function in glucose and metal ion transport. *Nat. Cell Biol.* **15,** 461–471
17. Gallon, M., Clairfeuille, T., Steinberg, F., Mas, C., Ghai, R., Sessions, R. B., Teasdale, R. D., Collins, B. M., and Cullen, P. J. (2014) A unique PDZ domain and arrestin-like fold interaction reveals mechanistic details of endocytic recycling by SNX27-retromer. *Proc. Natl. Acad. Sci. U.S.A.* **111,** E3604–E3613
18. Lauffer, B. E., Melero, C., Temkin, P., Lei, C., Hong, W., Kortemme, T., and von Zastrow, M. (2010) SNX27 mediates PDZ-directed sorting from endosomes to the plasma membrane. *J. Cell Biol.* **190,** 565–574
19. Nakagawa, T., and Asahi, M. (2013) β_1-Adrenergic receptor recycles via a membranous organelle, recycling endosome, by binding with sorting nexin27. *J. Membr. Biol.* **246,** 571–579
20. Bauch, C., Koliwer, J., Buck, F., Hönck, H. H., and Kreienkamp, H. J. (2014) Subcellular sorting of the G-protein coupled mouse somatostatin receptor 5 by a network of PDZ-domain containing proteins. *PLoS One* **9,** e88529
21. Lin, T. B., Lai, C. Y., Hsieh, M. C., Wang, H. H., Cheng, J. K., Chau, Y. P., Chen, G. D., and Peng, H. Y. (2015) VPS26A-SNX27 interaction-dependent mGluR5 recycling in dorsal horn neurons mediates neuropathic pain in rats. *J. Neurosci.* **35,** 14943–14955
22. Puthenveedu, M. A., Lauffer, B., Temkin, P., Vistein, R., Carlton, P., Thorn, K., Taunton, J., Weiner, O. D., Parton, R. G., and von Zastrow, M. (2010) Sequence-dependent sorting of recycling proteins by actin-stabilized endosomal microdomains. *Cell* **143,** 761–773
23. Vistein, R., and Puthenveedu, M. A. (2013) Reprogramming of G protein-coupled receptor recycling and signaling by a kinase switch. *Proc. Natl. Acad. Sci. U.S.A.* **110,** 15289–15294
24. Cao, T. T., Deacon, H. W., Reczek, D., Bretscher, A., and von Zastrow, M. (1999) A kinase-regulated PDZ-domain interaction controls endocytic sorting of the β_2-adrenergic receptor. *Nature* **401,** 286–290
25. Gage, R. M., Matveeva, E. A., Whiteheart, S. W., and von Zastrow, M. (2005) Type I PDZ ligands are sufficient to promote rapid recycling of G protein-coupled receptors independent of binding to *N*-ethylmaleimide-sensitive factor. *J. Biol. Chem.* **280,** 3305–3313
26. Cheloha, R. W., Gellman, S. H., Vilardaga, J. P., and Gardella, T. J. (2015) PTH receptor-1 signalling: mechanistic insights and therapeutic prospects. *Nat. Rev. Endocrinol.* **11,** 712–724
27. Drake, M. T., Shenoy, S. K., and Lefkowitz, R. J. (2006) Trafficking of G protein-coupled receptors. *Circ. Res.* **99,** 570–582
28. Srivastava, A., Gupta, B., Gupta, C., and Shukla, A. K. (2015) Emerging functional divergence of β-arrestin isoforms in GPCR function. *Trends Endocrinol. Metab.* **26,** 628–642
29. Walther, C., and Ferguson, S. S. (2013) Arrestins: role in the desensitization, sequestration, and vesicular trafficking of G protein-coupled receptors. *Prog. Mol. Biol. Transl. Sci.* **118,** 93–113
30. Vilardaga, J. P., Jean-Alphonse, F. G., and Gardella, T. J. (2014) Endosomal generation of cAMP in GPCR signaling. *Nat. Chem. Biol.* **10,** 700–706
31. Kotowski, S. J., Hopf, F. W., Seif, T., Bonci, A., and von Zastrow, M. (2011) Endocytosis promotes rapid dopaminergic signaling. *Neuron* **71,** 278–290
32. Irannejad, R., Tomshine, J. C., Tomshine, J. R., Chevalier, M., Mahoney, J. P., Steyaert, J., Rasmussen, S. G., Sunahara, R. K., El-Samad, H., Huang, B., and von Zastrow, M. (2013) Conformational biosensors reveal GPCR signalling from endosomes. *Nature* **495,** 534–538
33. Chauvin, S., Bencsik, M., Bambino, T., and Nissenson, R. A. (2002) Parathyroid hormone receptor recycling: role of receptor dephosphorylation and β-arrestin. *Mol. Endocrinol.* **16,** 2720–2732
34. Ferrari, S. L., Behar, V., Chorev, M., Rosenblatt, M., and Bisello, A. (1999) Endocytosis of ligand-human parathyroid hormone receptor 1 complexes is protein kinase C-dependent and involves β-arrestin2: real-time monitoring by fluorescence microscopy. *J. Biol. Chem.* **274,** 29968–29975
35. Sneddon, W. B., Bisello, A., Magyar, C. E., Willick, G. E., Syme, C. A., Galbiati, F., and Friedman, P. A. (2004) Ligand-selective dissociation of activation and internalization of the parathyroid hormone (PTH) receptor: conditional efficacy of PTH peptide fragments. *Endocrinology* **145,** 2815–2823
36. Vilardaga, J. P., Krasel, C., Chauvin, S., Bambino, T., Lohse, M. J., and Nissenson, R. A. (2002) Internalization determinants of the parathyroid hormone receptor differentially regulate β-arrestin/receptor association. *J. Biol. Chem.* **277,** 8121–8129
37. Ferrandon, S., Feinstein, T. N., Castro, M., Wang, B., Bouley, R., Potts, J. T., Gardella, T. J., and Vilardaga, J. P. (2009) Sustained cyclic AMP production by parathyroid hormone receptor endocytosis. *Nat. Chem. Biol.* **5,** 734–742
38. Calebiro, D., Nikolaev, V. O., Gagliani, M. C., de Filippis, T., Dees, C., Tacchetti, C., Persani, L., and Lohse, M. J. (2009) Persistent cAMP-signals triggered by internalized G-protein-coupled receptors. *PLoS Biol.* **7,** e1000172
39. Feinstein, T. N., Yui, N., Webber, M. J., Wehbi, V. L., Stevenson, H. P., King, J. D., Jr., Hallows, K. R., Brown, D., Bouley, R., and Vilardaga, J. P. (2013) Noncanonical control of vasopressin receptor type 2 signaling by retromer and arrestin. *J. Biol. Chem.* **288,** 27849–27860
40. Tsvetanova, N. G., and von Zastrow, M. (2014) Spatial encoding of cyclic AMP signaling specificity by GPCR endocytosis. *Nat. Chem. Biol.* **10,** 1061–1065
41. Gidon, A., Al-Bataineh, M. M., Jean-Alphonse, F. G., Stevenson, H. P., Watanabe, T., Louet, C., Khatri, A., Calero, G., Pastor-Soler, N. M., Gardella, T. J., and Vilardaga, J. P. (2014) Endosomal GPCR signaling turned off by negative feedback actions of PKA and v-ATPase. *Nat. Chem. Biol.* **10,** 707–709
42. Feinstein, T. N., Wehbi, V. L., Ardura, J. A., Wheeler, D. S., Ferrandon, S., Gardella, T. J., and Vilardaga, J. P. (2011) Retromer terminates the generation of cAMP by internalized PTH receptors. *Nat. Chem. Biol.* **7,** 278–284
43. Seaman, M. N. J. (2012) The retromer complex: endosomal protein recycling and beyond. *J. Cell Sci.* **125,** 4693–4702

44. Conway, B. R., Minor, L. K., Xu, J. Z., D'Andrea, M. R., Ghosh, R. N., and Demarest, K. T. (2001) Quantitative analysis of agonist-dependent parathyroid hormone receptor trafficking in whole cells using a functional green fluorescent protein conjugate. *J. Cell. Physiol.* **189,** 341–355
45. Huang, Z., Chen, Y., and Nissenson, R. A. (1995) The cytoplasmic tail of the G-protein-coupled receptor for parathyroid hormone and parathyroid hormone-related protein contains positive and negative signals for endocytosis. *J. Biol. Chem.* **270,** 151–156
46. Tawfeek, H. A., Qian, F., and Abou-Samra, A. B. (2002) Phosphorylation of the receptor for PTH and PTHrP is required for internalization and regulates receptor signaling. *Mol. Endocrinol.* **16,** 1–13
47. Alonso, V., Magyar, C. E., Wang, B., Bisello, A., and Friedman, P. A. Ubiquitination-deubiquitination balance dictates ligand-stimulated PTHR sorting. (2011) Ubiquitination-deubiquitination balance dictates ligand-stimulated PTHR sorting. *J. Bone Miner. Res.* **26,** 2923–2934
48. Romero, G., von Zastrow, M., and Friedman, P. A. (2011) Role of PDZ proteins in regulating trafficking, signaling, and function of GPCRs: means, motif, and opportunity. *Adv. Pharmacol.* **62,** 279–314
49. Ardura, J. A., Wang, B., Watkins, S. C., Vilardaga, J. P., and Friedman, P. A. (2011) Dynamic Na^+-H^+ exchanger regulatory factor-1 association and dissociation regulate parathyroid hormone receptor trafficking at membrane microdomains. *J. Biol. Chem.* **286,** 35020–35029
50. Wang, B., Bisello, A., Yang, Y., Romero, G. G., and Friedman, P. A. (2007) NHERF1 regulates parathyroid hormone receptor membrane retention without affecting recycling. *J. Biol. Chem.* **282,** 36214–36222
51. Geiser, M., Cèbe, R., Drewello, D., and Schmitz, R. (2001) Integration of PCR fragments at any specific site within cloning vectors without the use of restriction enzymes and DNA ligase. *BioTechniques* **31,** 88–92
52. Chaudhary, S., Pak, J. E., Gruswitz, F., Sharma, V., and Stroud, R. M. (2012) Overexpressing human membrane proteins in stably transfected and clonal human embryonic kidney 293S cells. *Nat. Protoc.* **7,** 453–466
53. Valdes, J. L., Tang, J., McDermott, M. I., Kuo, J. C., Zimmerman, S. P., Wincovitch, S. M., Waterman, C. M., Milgram, S. L., and Playford, M. P. (2011) Sorting nexin 27 protein regulates trafficking of a p21-activated kinase (PAK) interacting exchange factor (β-Pix)-G protein-coupled receptor kinase interacting protein (GIT) complex via a PDZ domain interaction. *J. Biol. Chem.* **286,** 39403–39416
54. Shi, H., Rojas, R., Bonifacino, J. S., and Hurley, J. H. (2006) The retromer subunit Vps26 has an arrestin fold and binds Vps35 through its C-terminal domain. *Nat. Struct. Mol. Biol.* **13,** 540–548
55. Ghai, R., Mobli, M., Norwood, S. J., Bugarcic, A., Teasdale, R. D., King, G. F., and Collins, B. M. (2011) Phox homology band 4.1/ezrin/radixin/moesin-like proteins function as molecular scaffolds that interact with cargo receptors and Ras GTPases. *Proc. Natl. Acad. Sci. U.S.A.* **108,** 7763–7768
56. Kahsai, A. W., Rajagopal, S., Sun, J., and Xiao, K. (2014) Monitoring protein conformational changes and dynamics using stable-isotope labeling and mass spectrometry. *Nat. Protoc.* **9,** 1301–1319
57. Nobles, K. N., Xiao, K., Ahn, S., Shukla, A. K., Lam, C. M., Rajagopal, S., Strachan, R. T., Huang, T. Y., Bressler, E. A., Hara, M. R., Shenoy, S. K., Gygi, S. P., and Lefkowitz, R. J. (2011) Distinct phosphorylation sites on the β_2-adrenergic receptor establish a barcode that encodes differential functions of β-arrestin. *Sci. Signal.* **4,** ra51
58. Haas, W., Faherty, B. K., Gerber, S. A., Elias, J. E., Beausoleil, S. A., Bakalarski, C. E., Li, X., Villén, J., and Gygi, S. P. (2006) Optimization and use of peptide mass measurement accuracy in shotgun proteomics. *Mol. Cell. Proteomics* **5,** 1326–1337
59. Balana, B., Maslennikov, I., Kwiatkowski, W., Stern, K. M., Bahima, L., Choe, S., and Slesinger, P. A. (2011) Mechanism underlying selective regulation of G protein-gated inwardly rectifying potassium channels by the psychostimulant-sensitive sorting nexin 27. *Proc. Natl. Acad. Sci. U.S.A.* **108,** 5831–5836
60. Case, D. A., Darden, T. A., Cheatham, T. E., 3rd, Simmerling, C. L., Wang, J., Duke, R. E., Luo, R., Merz, K. M., Pearlman, D. A., Crowley, M., Walker, R. C., Zhang, W., Wang, B., Hayik, S., Roitberg, A., *et al.* (2006) AMBER 9, University of California, San Francisco
61. Case, D. A., Darden, T. A., Cheatham, T. E., 3rd, Simmerling, C. L., Wang, J., Duke, R. E., Luo, R., Walker, R. C., Zhang, W., Merz, K. M., Roberts, B., Wang, B., Hayik, S., Roitberg, A., Seabra, G., *et al.* (2010) AMBER 11, University of California, San Francisco
62. Hornak, V., Abel, R., Okur, A., Strockbine, B., Roitberg, A., and Simmerling, C. (2006) Comparison of multiple Amber force fields and development of improved protein backbone parameters. *Proteins* **65,** 712–725
63. Berendsen, H. J. C., Postma, J. P. M., Vangunsteren, W. F., Dinola, A., and Haak, J. R. (1984) Molecular dynamics with coupling to an external bath. *J. Chem. Phys.* **81,** 3684–3690
64. Darden, T., York, D., and Pedersen, L. (1993) Particle mesh Ewald: an N·log(N) method for Ewald sums in large systems. *J. Chem. Phys.* **98,** 10089–10092
65. Ryckaert, J. P., Ciccotti, G., and Berendsen, H. J. C. (1977) Numerical integration of Cartesian equations of motion of a system with constraints: molecular dynamics of *n*-alkanes. *J. Comp. Phys.* **23,** 327–341
66. Wang, B., Yang, Y., and Friedman, P. A. (2008) Na/H exchange regulatory factor 1, a novel AKT-associating protein, regulates extracellular signal-regulated kinase signaling through a B-Raf-mediated pathway. *Mol. Biol. Cell* **19,** 1637–1645
67. Cushing, P. R., Fellows, A., Villone, D., Boisguérin, P., and Madden, D. R. (2008) The relative binding affinities of PDZ partners for CFTR: a biochemical basis for efficient endocytic recycling. *Biochemistry* **47,** 10084–10098
68. Roehrl, M. H. A., Wang, J. Y., and Wagner, G. (2004) A general framework for development and data analysis of competitive high-throughput screens for small-molecule inhibitors of protein-protein interactions by fluorescence polarization. *Biochemistry* **43,** 16056–16066
69. Syme, C. A., Friedman, P. A., and Bisello, A. (2005) Parathyroid hormone receptor trafficking contributes to the activation of extracellular signal-regulated kinases but is not required for regulation of cAMP signaling. *J. Biol. Chem.* **280,** 11281–11288
70. Bowman, S. L., Soohoo, A. L., Shiwarski, D. J., Schulz, S., Pradhan, A. A., and Puthenveedu, M. A. (2015) Cell-autonomous regulation of μ-opioid receptor recycling by substance P. *Cell Rep.* **10,** 1925–1936
71. Bowman, S. L., Soohoo, A. L., and Puthenveedu, M. A. (2015) Visualizing and quantitating sequence-dependent GPCR recycling. *Methods Cell Biol.* **130,** 333–345
72. Mahon, M. J. (2009) The parathyroid hormone 1 receptor directly binds to the FERM domain of ezrin, an interaction that supports apical receptor localization and signaling in LLC-PK1 cells. *Mol. Endocrinol.* **23,** 1691–1701
73. Vilardaga, J. P., Romero, G., Friedman, P. A., and Gardella, T. J. (2011) Molecular basis of parathyroid hormone receptor signaling and trafficking: a family B GPCR paradigm. *Cell Mol. Life Sci.* **68,** 1–13
74. Sneddon, W. B., Syme, C. A., Bisello, A., Magyar, C. E., Weinman, E. J., Rochdi, M. D., Parent, J. L., Abou-Samra, A. B., and Friedman, P. A. (2003) Activation-independent parathyroid hormone receptor internalization is regulated by NHERF1 (EBP50). *J. Biol. Chem.* **278,** 43787–43796
75. Zimmerman, S. P., Hueschen, C. L., Malide, D., Milgram, S. L., and Playford, M. P. (2013) Sorting nexin 27 (SNX27) associates with zonula occludens-2 (ZO-2) and modulates the epithelial tight junction. *Biochem. J.* **455,** 95–106
76. Miesenböck, G. (2012) Synapto-pHluorins: genetically encoded reporters of synaptic transmission. *Cold Spring Harb. Protoc.* **2012,** 213–217
77. Mayle, K. M., Le, A. M., and Kamei, D. T. (2012) The intracellular trafficking pathway of transferrin. *Biochim. Biophys. Acta* **1820,** 264–281
78. Cong, M., Perry, S. J., Hu, L. A., Hanson, P. I., Claing, A., and Lefkowitz, R. J. (2001) Binding of the β_2-adrenergic receptor to *N*-ethylmaleimide-sensitive factor regulates receptor recycling. *J. Biol. Chem.* **276,** 45145–45152
79. Song, I., Kamboj, S., Xia, J., Dong, H., Liao, D., and Huganir, R. L. (1998) Interaction of the *N*-ethylmaleimide-sensitive factor with AMPA receptors. *Neuron* **21,** 393–400
80. Nishimune, A., Isaac, J. T., Molnar, E., Noel, J., Nash, S. R., Tagaya, M., Collingridge, G. L., Nakanishi, S., and Henley, J. M. (1998) NSF binding to GluR2 regulates synaptic transmission. *Neuron* **21,** 87–97
81. Wang, Y., Lauffer, B., Von Zastrow, M., Kobilka, B. K., and Xiang, Y. (2007) *N*-Ethylmaleimide-sensitive factor regulates β_2 adrenoceptor trafficking and signaling in cardiomyocytes. *Mol. Pharmacol.* **72,** 429–439
82. Tawfeek, H. A., and Abou-Samra, A. B. (2004) Important role for the

V-type H^+-ATPase and the Golgi apparatus in the recycling of PTH/PTHrP receptor. *Am. J. Physiol. Endocrinol. Metab.* **286,** E704–E710
83. Garrido, J. L., Wheeler, D., Vega, L. L., Friedman, P. A., and Romero, G. (2009) Role of phospholipase D in parathyroid hormone type 1 receptor signaling and trafficking. *Mol. Endocrinol.* **23,** 2048–2059
84. van Dam, E. M., Ten Broeke, T., Jansen, K., Spijkers, P., and Stoorvogel, W. (2002) Endocytosed transferrin receptors recycle via distinct dynamin and phosphatidylinositol 3-kinase-dependent pathways. *J. Biol. Chem.* **277,** 48876–48883
85. Arighi, C. N., Hartnell, L. M., Aguilar, R. C., Haft, C. R., and Bonifacino, J. S. (2004) Role of the mammalian retromer in sorting of the cation-independent mannose 6-phosphate receptor. *J. Cell Biol.* **165,** 123–133
86. Alonso, V., and Friedman, P. A. (2013) Minireview: ubiquitination-regulated G protein-coupled receptor signaling and trafficking. *Mol. Endocrinol.* **27,** 558–572
87. Ryu, J. K., Min, D., Rah, S. H., Kim, S. J., Park, Y., Kim, H., Hyeon, C., Kim, H. M., Jahn, R., and Yoon, T. Y. (2015) Spring-loaded unraveling of a single SNARE complex by NSF in one round of ATP turnover. *Science* **347,** 1485–1489
88. Chan, A. S. M., Clairfeuille, T., Landao-Bassonga, E., Kinna, G., Ng, P. Y., Loo, L. S., Cheng, T. S., Zheng, M., Hong, W., Teasdale, R. D., Collins, B. M., and Pavlos, N. J. (2016) Sorting Nexin 27 couples PTHR trafficking to retromer for signal regulation in osteoblasts during bone growth. *Mol. Biol. Cell* **27,** 1367–1382
89. Lee, S., Chang, J., and Blackstone, C. (2016) FAM21 directs SNX27-retromer cargoes to the plasma membrane by preventing transport to the Golgi apparatus. *Nat. Commun.* **7,** 10939
90. Peng, Y., Ayaz-Guner, S., Yu, D., and Ge, Y. (2014) Top-down mass spectrometry of cardiac myofilament proteins in health and disease. *Proteomics Clin. Appl.* **8,** 554–568